University of Stavanger

Faculty of Science and Technology

BACHELOR THESIS

Study program/Specialization: Petroleum Technology	Spring semester, 2021 Open
Author: Haugland, Kornelius	 (Author's signature)
Faculty supervisor: Rabenjafimanantsoa, Hermonja A. Co-supervisor: Time, Rune W.	
Thesis title: Flow of viscoplastic fluids in horizontal pipe	
Credits (ECTS): 20	
Key words: - Drilling fluids - Yield stress fluids - Carbopol - Herschel-Bulkely fluids - Velocity profile - Flow loop - Particle Image Velocimetry	Pages: 66 + enclosure: 24 Stavanger, 15.05.2021

Flow of viscoplastic fluids in a horizontal pipe

Bachelor thesis spring 2021

Kornelius Haugland

Department of Energy and Petroleum Engineering

Faculty of Science and Technology

University of Stavanger

15.05.2021

Summary

The aim of this thesis was to study the flow of viscoplastic fluids in a horizontal pipe. Rheology of the fluid was measured using two different rheometers, one of them being a V-G meter, which is more commonly used in petroleum field operations. The other was an Anton Paar MCR 302, which is considered to be more accurate, however it is not generally suitable for oilfield application. Emphasis of this thesis is on defining the yield point for these viscoplastic fluids executed with these rheometers. A flow loop system was built for the fluids for this particular study. Moreover, this system provided possibilities for pressure measurements and velocity profile examination by using Particle Image Velocimetry (PIV) technique. Prior to the tests, water measurements were carried out. These measurements served as reliable data for comparisons and calibration of the system.

The fluid measurements performed within this system were carried out on three different weight% of Carbopol mixed with distilled water. The rheology was examined using the MCR 302 before and after performing these measurements within the flow loop system. By comparing these results, it was evident that the properties of the fluids changed. Furthermore, the longer time the fluids were subjected in this system, the more the properties were altered. The result of the highest weight% of Carbopol is characterized by a relatively large change due to complications when performing the Particle Image Velocimetry measurements.

The comparison of the selected velocity profiles and summary for yield stress values obtained from the MCR 302 are displayed below in Figure 1 and Table 1 respectively. The velocity profiles are represented as a sixth-degree polynomial, and Table 1 provides values for the yield stress for the three viscoplastic fluids examined based on a log-log plot for the data points.

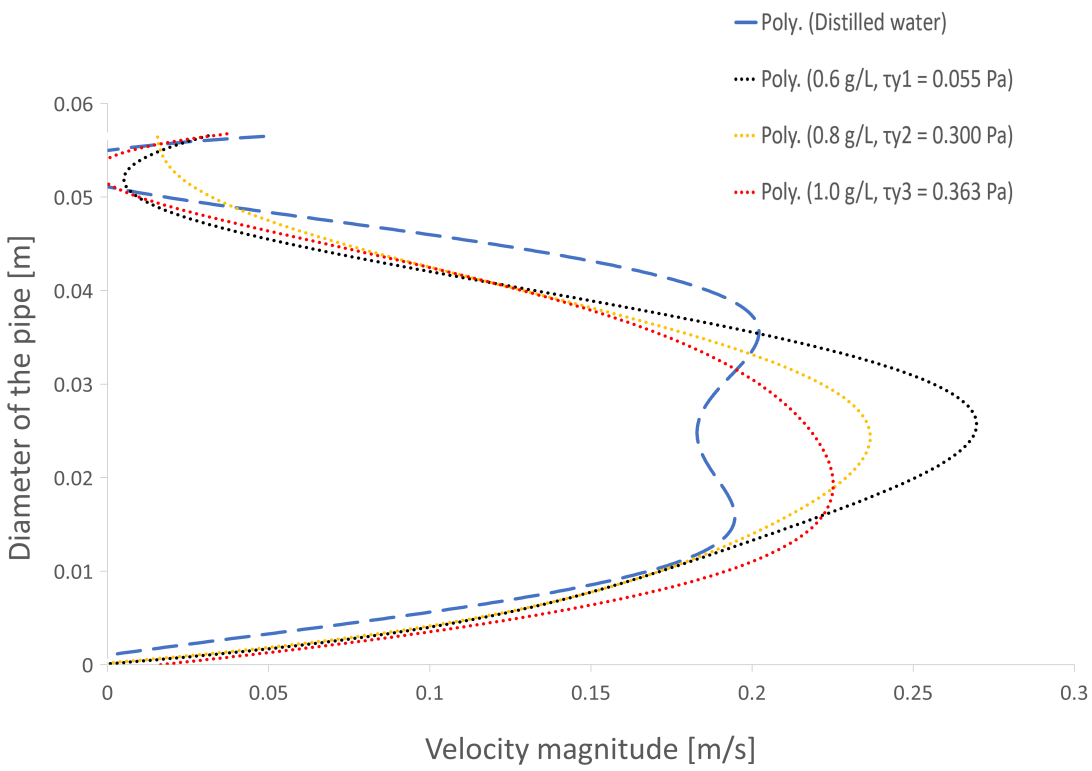

Figure 1: Velocity profiles of distilled water, and Carbopol concentrations of 0.6 g/L, 0.8 g/L and 1.0 g/L combined as sixth degree polynomial. Measured at a flow rate of $\approx 15.14 L/min$.

Table 1: Yield stresses for each fluid based on the values from the log-log plot displayed in Figure 4.9, before and after running the experiments.

Carbopol mixtures	**0.6 g/L**	**0.8 g/L**	**1.0 g/L**
Yield Stress, τ_y, initially $[Pa]$	0.116	0.368	0.946
Yield Stress, τ_y, after system $[Pa]$	0.055	0.300	0.363

Contents

Acknowledgement

First and foremost we would like to express our gratitude to our supervisor Hermonja A. Rabenjafimanantsoa, Senior Engineer at the University of Stavanger. Not only has he provided us with this golden opportunity with an experimental task we found interesting, but he has been by our side throughout the entire project. He has shared his knowledge and provided excellent guidance which we highly appreciate. He showed great enthusiasm and interest in the project and made hours spent in the lab fly by.

A huge thanks to Kim Andre Nesse Vorland for taking time out of his days to teach us how to use the MCR 302 rheometer. We would also like to express our gratitude to Hans Joakim Skadsem who provided us with help in interpreting data points from the rheometers, and how to perform Herschel-Bulkey approximation using Excel.

This bachelor thesis concludes the completion of a 3-year long petroleum engineering study; therefore we would like to take this opportunity to thank our families for their encouragements throughout this journey.

Nomenclature

Abbreviations

0.6 g/L	0.6 g Carbopol Ultrez 10 and 3.5 mL 5% NaOH per L distilled water
0.8 g/L	0.8 g Carbopol Ultrez 10 and 5.0 mL 5% NaOH per L distilled water
1.0 g/L	1.0 g Carbopol Ultrez 10 and 6.5 mL 5% NaOH per L distilled water
API	American Petroleum Institute
AS	Amplitude Sweep
AVI	Audio Video Interleave
ASCII	American Standard Code for Information Interchange
CSR	Controlled Shear Rate
CSS	Controlled Shear Stress
DCC	Discrete Cross-Correlation
H-B	Herschel-Bulkley
ISO	International Standards Organization
IW	Interrogation Window
LED	Light emitting diode
MCR 302	Modular Compact Rheometer 302
PIV	Particle Image Velocimetry
PVC	Polyvinyl chloride
RPM	Revolutions per minute
SI	International System of Units
TIFF	Tag Image File Format
VP	Viscoplastic
V-G	Viscosity-Gel

Roman letters

A	Shear area
a	MCR 302 gap f_t
Gray- scale value at t	
h	Shear gap
D	Diameter
ID	Inner diameter
k	Consistency factor
L	Length pipe
M	number of pixels in IW
m_x	x- component of the displacement factor
n	Flow behaviour index
n_1	Refractive index 1
n_2	Refractive index 2
n_y	y- component of the displacement factor
F	Shear force
P	Pressure
P_r	Incident ray
Q	Refracted ray
r	Radius of unyielding plug
R	Radius
R^2	Coefficient of regression
Re	Reynolds number
s	Length of deflection
t	Time
Δt	Time interval
u	Velocity magnitude
v	Velocity
V_{avg}	Mean speed of fluid
v_x	Horizontal velocity
v_y	Vertical velocity
v_1	Velocity in medium 1
v_2	Velocity in medium 2
$\bar{x}$	Common displacement
y	Shear deformation

Greek letters

α	Angle
Δ	Change in variable
γ	Shear rate
μ	Dynamic viscosity
μ_p	Plastic viscosity
ν	Kinematic viscosity
ρ	Density
τ	Shear stress
τ_y	Yield point
τ_W	Wall shear stress
θ	Dial reading
θ_1	Ray entry angle
θ_2	Ray exit angle

List of Figures

List of Tables

Chapter 1

Introduction

Viscoplastic fluids are encountered in both industry, such as in cosmetics, food or petroleum, and also in day-to-day items including toothpaste, margarine or paint [1]. As this is a bachelor thesis performed at the department of Energy and Petroleum Engineering the main focus is the utilization of viscoplastic fluids in the petroleum industry. Drilling fluids, cement slurries and heavy oils are examples of viscoplastic fluids met in this industry.

1.1 Background

This section presents an overview of the thesis, objectives and brief characterizing of viscoplastic fluids. Additionally, an overview of the thesis' structure is provided.

Rheological measurements will be carried out on Carpool dispersed in multiple aqueous solutions. The construction of an experimental setup representing a horizontal pipe will also be build in order to get an approximation of the compositions' flow regimes. This will be carried out using Particle Image Velocimetry (PIV). Additionally, pressure test will be performed in this system.

1.1.1 Utilization and problems

Viscoplastic fluids are rheologically characterized as a shear thinning material, with a key property being a yield stress. Shear thinning means that the shear stress will decrease by an increase of shear rate. The yield stress is the threshold for where the viscoplastic material goes from a solid-like material to a flowing one. These properties allow higher flow rates of drilling fluids in drilling operations and make excellent transporters of drill cuttings. However, according to [2], yield stress fluids in drilling operations also lead to complications. After the displacement of the viscoplastic fluid, it is possible that fluid may persist at the duct wall, if the yield stress is sufficiently large [3]. They may also get stuck under transportation and/or need to be cleaned out.

By taking viscoplastic fluids' useful properties, its corresponding issues and lack of extensive research into account, there seems to be a gap for needed work and research. This thesis is motivated accordingly and will hopefully fill this gap ever so slightly.

1.1.2 Scope and objective

This thesis is purely experimental and will aim to study viscoplastic fluids' rheological behaviour, properties with yield stress being the main focus. Three different concentrations of Carbopol solutions will be examined. They will be compared to each other, in addition to water. The properties of the fluids are going to be studied by using both a V-G rheometer, and a MCR 302 rheometer. The flow loop will also be examined in a horizontal cylindrical pipe which is a part of a nearly closed loop. A Particle Image Velocimetry (PIV) test will be carried out to study the velocity profile of the fluid in a determined polyline. Furthermore, the pressure differences within the pipe will be examined.

The thesis consists of 5 chapters and 2 appendices which includes additional information.

Chapter 1 provides an insight in what this thesis will entail, the motivation behind the topic and an overview of the thesis as a whole.

Chapter 2 provides the foundation for the thesis and includes theory and definitions of fluids and rheological models.

Chapter 3 describes in detail of the experimental setup and the procedures for the experiments.

Chapter 4 addresses the results and discussions from the previous chapter. These will be examined, explained and discussed.

Chapter 5 is the conclusion for the project.

Appendix A includes additional information from experiments and measurements.

Appendix B provides additional illustrations relevant for the thesis.

Chapter 2

Theoretical study

This chapters provides an in-depth coverage of relevant terms, models and measurement techniques.

2.1 Rheology

Rheology is the science of deformation and flow under applied force [4]. Important variables within rheology, such as forces, deflections and velocities connect it to physics and physical chemistry. The term "rheology" stems from Greek and is translated to "flow science". However, rheology touches on more than just flow behavior for liquids, the deformation behaviour of solids is also a key point. Applied shear forces to some solids would lead to a large deformation and cause them to flow [4].

2.1.1 Rheometry and Viscometry

Rheometry is a general term that refers to experimental methods in measurement of rheological properties. Viscometry is a narrower term and refers to measurements of viscosity [5]. Some important terms within rheometry are shear stress, shear rate, shear deformation and viscosity. Furthermore, these terms are central in this paper and understanding what they are is therefore important. [6] provides good definitions and information around these using the two-plates model, as shown in Figure 2.1.

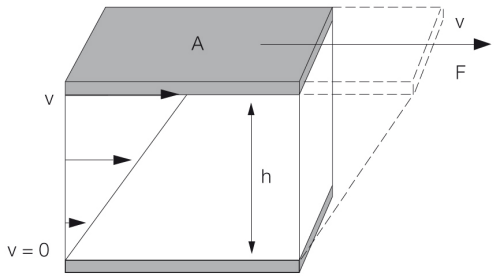

Figure 2.1: Calculation of shear stress using two-plate model with shear area, A, gap width, h, shear force F, and velocity, v [7].

The model consist of two plates, where the lower one is stationary, while the other one moves when shear forces acts upon the sample wedged between them. The two-plate model will in the following subsections be used to describe shear stress, shear rate and shear deformation.

Shear stress

Shear stress is defined by the equation

$$\tau = \frac{F}{A} \tag{2.1}$$

Here τ is shear rate [Pa], F is shear force [N] and A is the shear area [m^2]. The unit for shear stress is [N/m^2], which is equivalent to [Pa]. A rheometer supplies torque to a fluid, which in turn creates a shear stress. This is measured at each measuring point.

Shear rate

Shear rate is defined by the equation

$$\gamma = \frac{v}{h} \tag{2.2}$$

γ indicates the shear rate; v and h represent the velocity [m/s] and shear gap [m] respectively. It is defined as the rate for which a sample is deformed by progressively applying shear, while keeping a constant volume. The unit for shear rate is [$1/s$], and is more usually written as [s^{-1}]. This is also known as the inverse of a second or reciprocal seconds. A rheometer logs the velocity as rotational speed. Considering that radial distance is a parameter of rotational speed, knowing the shear gap width is crucial.

Shear deformation

Shear deformation, also known as shear strain is a dimensionless term which quantifies the extent of deformation caused by shear stress, usually stated as a percentage. It is defined by the equation

$$y = \frac{s}{h} \tag{2.3}$$

y is the shear deformation [%], s is the length of deflection for the top plate [m] and h represent the shear gap [m].

Viscosity

Viscosity is the measurement of a fluid's internal resistance to flow [8]. It is usually dependant on both the fluids composition, temperature and pressure. Viscosity is a wide term and is often divided into different types of viscosity.

Dynamic viscosity is also known as absolute viscosity or shear viscosity. It is the ratio of shear stress to the velocity gradient, or shear rate, in a fluid. [9].

$$\mu = \frac{\tau}{\gamma} \tag{2.4}$$

This equation is derived from Newton's second law of motion, which states $F = ma$. The SI unit for viscosity is pascal seconds $[Pa \times s]$. However, it is rarely used in scientific writing. A more commonly used unit for viscosity is the dyne second per square centimetre $[dynes/cm^2]$, also known as poise [10].

Kinematic viscosity is the ratio of dynamic viscosity to its density, given that temperature and pressure remain constant. [9].

$$\nu = \frac{\mu}{\rho} \tag{2.5}$$

The unit for kinematic viscosity in SI units is $[m^2/s]$. However, it is impractically large and hardly ever used. A more common unit is $[mm/s]$ which is a smaller variant of stokes, $[cm/s]$. Kinematic viscosity is a measure of the resistance of flow, under the influence of gravity [10].

Apparent viscosity is the viscosity value for a fluid at a certain shear rate [9]. All fluids can be characterized as Newtonian or Non-Newtonian, depending on its rheological properties. For Newtonian fluids, the viscosity is constant for all shear rates, as opposed to for Non-Newtonian fluids. Therefore, it is important to specify at what shear rate the viscosity was determined.

2.1.2 Newtonian fluids

Newtonian fluids, or ideally viscous, are the most basic model for fluid that takes viscosity into account. The shear stress for such a fluid will increase linearly by an increase of shear stress, passing through the origin. There are only a few liquids or gasses that can be assumed to be fully Newtonian. Water is the most common Newtonian fluid. The model is named after Sir Isaac Newton, who described the flow behaviour for such fluids by equation 2.4.

2.1.3 Non-Newtonian fluids

Also known as shear-dependant fluid is a generic term for all fluids that doesn't fit the Newtonian model. Contrary to Newtonian fluids, the viscosity is dependant on the shear rate. Additionally, it often consists of particles or polymers which provides the fluids with various properties. To differentiate between the fluids with different properties they are often divided into 3 groups: Plastic, Pseudoplastic and dilatant fluids. Plastic fluids describe fluids that are characterized by a yield stress. Pseudoplastic and dilatant describe shear thinning and shear thickening fluids respectively [11]. Most drilling fluids are either plastic or pseudoplastic, while cement paste is a typical example of a shear thickening fluid. Figure 2.2 shows a brief overview of these fluids.

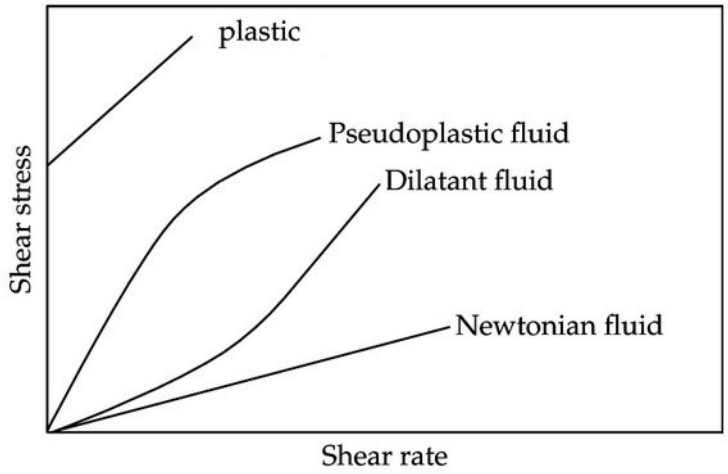

Figure 2.2: Newtonian and Non-Newtonian overview. Adapted from [12].

Viscoplastic fluids

Upon mixing Carbopol with water, the liquid goes from being Newtonian, to a Non-Newtonian viscoplastic fluid. Viscoplastic fluids are characterized by yield stress, τ_y, and a shear thinning quality. Yield stress is the critical value of needed shear stress applied before the fluid will start to flow. If not exceeded the fluid will show solid-like behaviour, as opposed to viscoelastic, which will show elastic properties until the yield threshold is reached. This specific property makes viscoplastic fluids particularly good in carrying the cuttings out since it is rigid and will not deform in contact with them. The amount of yield stress for a solution is dependant on molecular weight of the polymers. A higher molecular weight provides more entanglement and increases the resistance of the fluid. Moreover, it increases the viscosity of the fluid. Fluids consisting of a lower molecular weight tend to flow easier [13]. Shear thinning means the fluid will get a lower viscosity as more shear stress is applied. Viscoplastic fluids' flow are also history independent. It will not deform, nor will its qualities be affected by previous stress applied. This means that for a value of shear stress it is only dependent of the corresponding value of shear rate and vice versa.

Carbopol is a synthetic polymer of acrylic acid and will therefore affect the mixture by lowering the pH value. This is counteracted by an addition of NaOH, which leads to a decrease of free H+ ions [1]. Exposing drilling equipment to fluids either too high on the alkaline range or too low on the acidic range will damage the equipment and decrease its lifespan. Another property provided by the Carbopol polymer is gelling. It occurs when the fluid is left to rest and causes an increase in viscosity and turns the fluid more solid-like. Gelling is similar to yield stress, the difference is that gels are a measure of static forces, while yield-point is a measure of dynamic attractive forces [14]. Figure 2.3 illustrates the behaviour of particles for shear thinning polymer solutions.

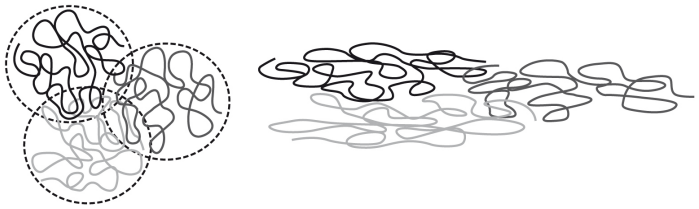

Figure 2.3: Left shows particles in suspension, right shows particles under shear [15]

The left side shows the entanglement of long polymer molecules and how they form ball-like shapes at rest. The right side shows how shear affects these formations. Under shear, the entanglements will unfold, stretch and align with the shear orientation. Individual molecules provide a weaker flow resistance than entangled superstructures [16]. Hence, increase in shear rate leads to a decrease of the fluids viscosity. The result is a shear thinning flow behaviour. [16].

2.1.4 Flow profiles in cylindrical pipes

It is easy to measure the flow rate of a fluid running through a system, but the distribution of velocity of particles depends on whether the flow is laminar or turbulent. As for many other engineering fields that includes fluid dynamics, the flow profile is very important in the petroleum industry. They are a decisive factor for how the fluids are transported through the drill string, the reservoir, and the annulus. The theoretical flow profiles are often idealised, and a combination of them will in practical situations be more realistic.

Reynolds number

By calculating the Reynolds number and using it in combination with the frictional factor of a pipe, one can get a good approximation of the flow profile. Reynolds number represents the ratio between inertial- and viscous forces. The number is dependent on the diameter of the pipe, the fluids flow rate, its viscosity and the density of the fluid.

$$Re = \frac{\rho V_{avg} D}{\mu} \tag{2.6}$$

Where Re is the unitless Reynolds number, V_{avg} is mean speed of the fluid in $[m/s]$ and D is the diameter of the pipe in $[m]$.

Flows with $Re < 2300$ through a pipe can for practical purposes be assumed to be laminar. However, when $Re > 4000$ it can be assumed to be turbulent. These values will of course depend on the friction factor of the pipe. For values between these two limits, the flow is in a transitional state going between laminar and turbulent. [17]

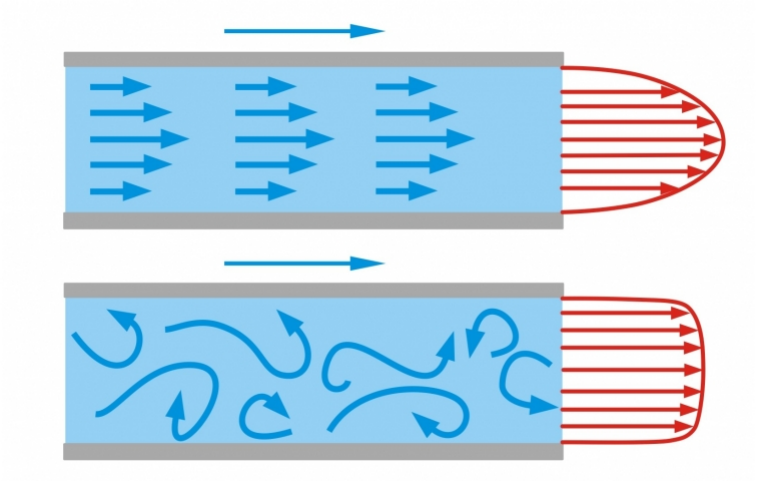

Figure 2.4: Velocity- distributions and profiles for laminar (top) and turbulent (bottom) flow regimes [18].

Laminar Flow

Laminar flow is characterized by a velocity profile of a longer parabolic shape similar to the first profile in Figure 2.4. The velocity of the fluid is largest in the centre and decreases towards the pipe wall. It is associated with a lower value of Reynolds number, making it a typical flow profile for fluids moving slow or fluids with higher viscosity. Using an average value for the velocity of the fluid is more convenient than determining the velocity for the fluid in each part of the pipe. This can be calculated by dividing the flow rate by the area of the pipe.

Turbulent flow

A turbulent profile is categorized by irregular movement of the flow. The presence of so called "eddies", which are the curled velocity vectors in Figure 2.4, are good indicators of such a flow. Most naturally occurring flows are considered turbulent as laminar flow requires really specific circumstances [19]. The Reynolds number for turbulent flow profiles are high. Their velocity magnitude profiles are usually flat, giving them a plug-like profile. Turbulent flows in pipes will have a laminar sublayer close to the boundary. This occurs because of the decrease in speed from frictional forces lowers Re enough to sustain a laminar profile [17].

The transition from a laminar to a turbulent flow will take place when the inertial forces in the flow start to dominate the viscosity [20]. When increasing the flow rate of the laminar flow, the magnitude of the velocity profile will increase until the critical *Re* value for turbulent transformation is reached. An illustration of the progressive velocity curve by increasing Reynolds number can be seen in Figure 2.5.

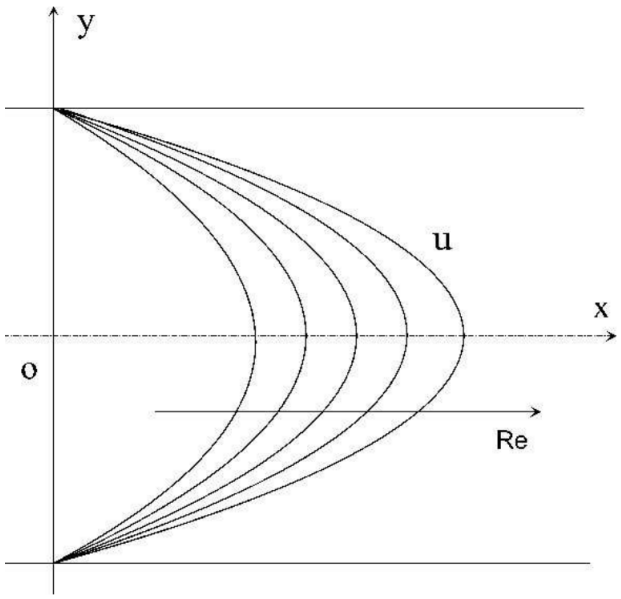

Figure 2.5: Effect of Reynolds number on an arbitrary, Newtonian velocity curve [21].

Plug profile

A plug profile is an idealized velocity profile which is often associated with turbulence. It is a uniform profile where the velocity of the fluid is equal throughout the cross section of the pipe, except close to pipe walls. To achieve plug flow this sublayer need to be much thinner than the diameter of the pipe. The irregularities and seemingly random distributed velocity vectors add up to a uniform and smooth velocity profile where only the laminar sublayer prevents it from being a straight line [22].

A plug-like velocity profile can also be drawn for a yield stress fluid in the laminar regime. An illustration of such profile can be found in Figure 2.6. This occurs because the fluid's yield strength is greater than the shear stress applied. This keeps it from obtaining the parabolic shape that is typical for Newtonian fluids. The flat surface is called the unyielding plug which acts as a solid-like block that doesn't mix. The radius of the plug can in combination with the wall shear stress be used to calculate the yield stress of the fluid [23].

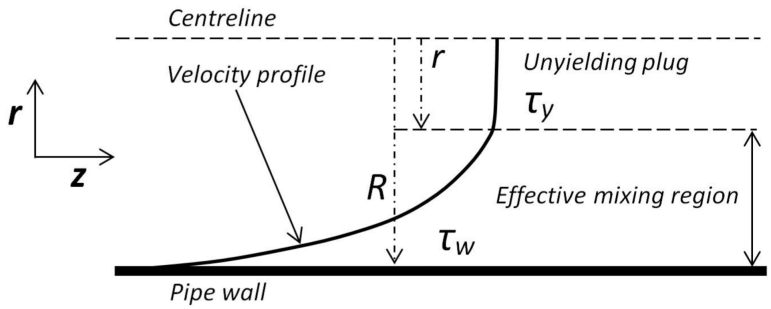

Figure 2.6: Lower half of the velocity profile of a yielding fluid [24].

Yield can be expressed as

$$\tau_y = \tau_W \left(\frac{r}{R} \right) \tag{2.7}$$

Where τ_W is the wall shear stress in $[Pa]$, which is equal to the velocity profile gradient $\frac{\partial u}{\partial y}$. R is the radius of the pipe and r is the radius of the unyielding plug, both in $[m]$.

The plugged profile makes yielding fluids suitable for drilling purposes. The plug-like flow allows for higher velocities closer to the formation, which in turn leads to better cuttings removal and transport.

Hydrodynamic entrance length

When running a fluid through a horizontal pipe it takes a certain length from the inlet before the flow reaches its fully developed flow profile. This length is called the hydrodynamic entrance length. This will be important for placement of measuring instruments such as flow meter, pressure sensors and camera for PIV. According to [25], assuming a length of 10×diameter would yield sufficient results for longer pipes.

From the inlet, an irrotational flow enters the pipe where there is a uniform distribution of particle velocity, and viscous effects are absent. Further, a viscous boundary-layer is gradually increasing in size until it covers the entire pipe. As the viscous boundary grows the flow will be slowed near the wall from friction, until the final velocity profile is reached.

The pressure gradient will also be significantly affected by the entrance length selected. After the fluid has passed the inlet with high pressure, the pressure will initially decrease rapidly. The pressure gradient will not reach a constant until the profile is entirely developed [26].

2.2 Rheological Instruments

Several instruments can be used to determine a fluid's rheological properties. In this section the instruments that were used for this thesis will be presented.

2.2.1 V-G meter

The V-G meter is a viscometer that examines the relationship between shear stress and shear rate for a fluid. It has the ability to measure both the viscosity and gel, hence the name "V-G", and studies the fluids behaviour inside annular space. The device consists of a cylindrical rotor sleeve, a bob that is submerged in the liquid and a torsion spring. It is operated by filling up a small container with 400 mL mixed viscoplastic fluid. The rheometer supplies shear rates at 7 different set rotational speeds, which easily can be alternated between. The conversion between RPM and shear rate is applied in accordance with API and ISO specifications [27] and is defined by

$$\gamma = RPM \times 1.703 \tag{2.8}$$

The unit for 1 dial reading corresponding to the shear rates are 1 $lbf/100ft^2$, or 0.511 Pa in SI units [27]. The viscosity measurements are made by the outer cylinder causing a viscous drag on the fluid by rotating at one of these set rotational speeds. This drag creates torque on the bob inside the cylinder, which is transmitted to a precision spring where the deflection of the fluid is measured [28]. Figure 3.5 provides an outline of the components for this viscometer.

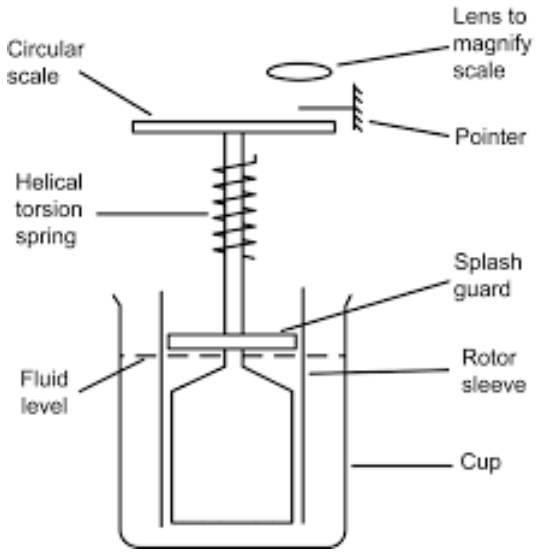

Figure 2.7: Components of the V-G meter [29].

2.2.2 Anton Paar MCR 302 Rheometer

The MCR 302 is a more advanced way of measuring a fluid's rheological properties. As opposed to the V-G meter, the MCR 302 rheometer is able to study the properties for fluids in a much greater degree. Especially when considering yield stress, as the MCR 302 is able to collect data points with shear rates considerably lower than that of the V-G meter. This makes it possible to pinpoint far more accurately were the fluid goes from showing solid-like behaviour to undergoing unrecoverable deformation. The MCR 302 has integrated thermal management [30], which makes it possible to obtain full control of a fluid's temperature throughout the testing. Temperature affects as previously mentioned a fluid's viscosity, and by being able to disregard any temperature deviation is a great advantage.

2.3 Rheological Models

Rheological models are used to approximate fluids' behaviour. In this thesis it was desired to describe the different concentrations by comparing each mixtures' shear stress against its shear rate, and then calculating its yield point. Several models do this, so finding the one that fit viscoplastic fluids the best was of great importance. The fitting of such fluids to various rheology models are well described in [31]. It was found that the Herchel-Bulkley model gives a good approximation of this fluid's behaviour. The Herchel-Bulkley model has been the standard industry model for these types of non- Newtonian fluids since the 1990s. Before that Bingham and power law was most frequently used. The Herschel-Bulkley model is a combination of its two predecessors but eliminates their biggest weaknesses [2].

2.3.1 Bingham plastic model

The Bingham plastic model describes shear stress by only using the two parameters yield stress and plastic viscosity.

$$\tau = \mu_p(\gamma) + \tau_y \tag{2.9}$$

Where the plastic viscosity, μ_p, is described as difference between readings at 600- and 300 RPM on the V-G meter. The yield point is approximated as the difference between the reading at 300 RPM and the plastic viscosity [32].

A Bingham plastic can be described as a material that acts as a solid until it reaches a critical shear stress and acts as a liquid. After this threshold is reached, the shear stress to shear rate curve is linear. The plastic viscosity is then the material's ability to flow freely. In drilling, lower plastic viscosity translates to the capability of drilling at a higher speed. A high yield point demands higher pump pressure. To get the desired drilling fluid one would balance between these two parameters [33].

The main problem with the Bingham plastic model is the assumption of the gradient for the shear rate versus shear stress is constant. When using a rheometer like

the V-G meter, the gradient is often based on measurements done at 300- and 600 RPM [32]. The linear assumption means that values at both low and high shear rates will often deviate from measured values in a fluid.

2.3.2 Power law model

In the Power law model, the shear rate versus shear stress curve has an exponential equation, and uses the two parameters k and n:

$$\tau = k\big(\gamma\big)^n \tag{2.10}$$

Where k is the consistency factor in $[Pa \times s^n]$ which gives an indication of the viscosity, and n is the unitless flow behaviour index which describes the effect of regulating shear stress.

V-G readings at 300- and 600 RPM are commonly used for this model as well [32], however it erases some of the Bingham plastic model's flaws by accounting for shear-thinning ($n < 1$) or shear-thickening ($n > 1$) behaviour of the fluid. Using this model one would get fairly good results for lower shear rates. Although, in the absence of a yield point the model's upper boundary would be far lower than the measured data for a shear thinning fluid [34].

2.3.3 Herschel-Bulkley

The Herschel-Bulkley model accounts for the most obvious flaws from the Bingham and Power law models by including a third parameter. This model provides a more accurate representation of viscoplastic fluid's behaviour. An additional reading for shear stress is also present in this model. This is measured at 3 RPM and is used to approximate yield point [32]. The H-B model defines shear stress by

$$\tau = \tau_y + k\big(\gamma\big)^n \tag{2.11}$$

H-B by least square method

In this thesis the yield point was particularly important, and a better approximation than the reading at 3 RPM was therefore preferable. An alternative procedure when using the Herschel-Bulkley method was then found, where additional testing and calculations yielded a more accurate model. This procedure demands more inputs in order to work properly, but given enough values for shear stress it gets even more precise than the standard model. It does this by utilizing the least square method to approximate each of the three parameters.

The least square method is commonly used in regression analysis in order to get the best fitting curve for a set of data. By making the squared difference between the Herschel-Bulkley model and the measured data as small as possible for the entire data set, you will get a good estimate of the true curve. A more thoroughly description of the procedure will be given in section 4.1.1.

Velocity profile of a H-B fluid

As described in section 2.1.4 a yield stress fluid will get a plugged velocity profile also in the laminar flow regime. Illustrated by Figure 2.8, increasing the shear-thinning exponent n will make the plug velocity decrease.

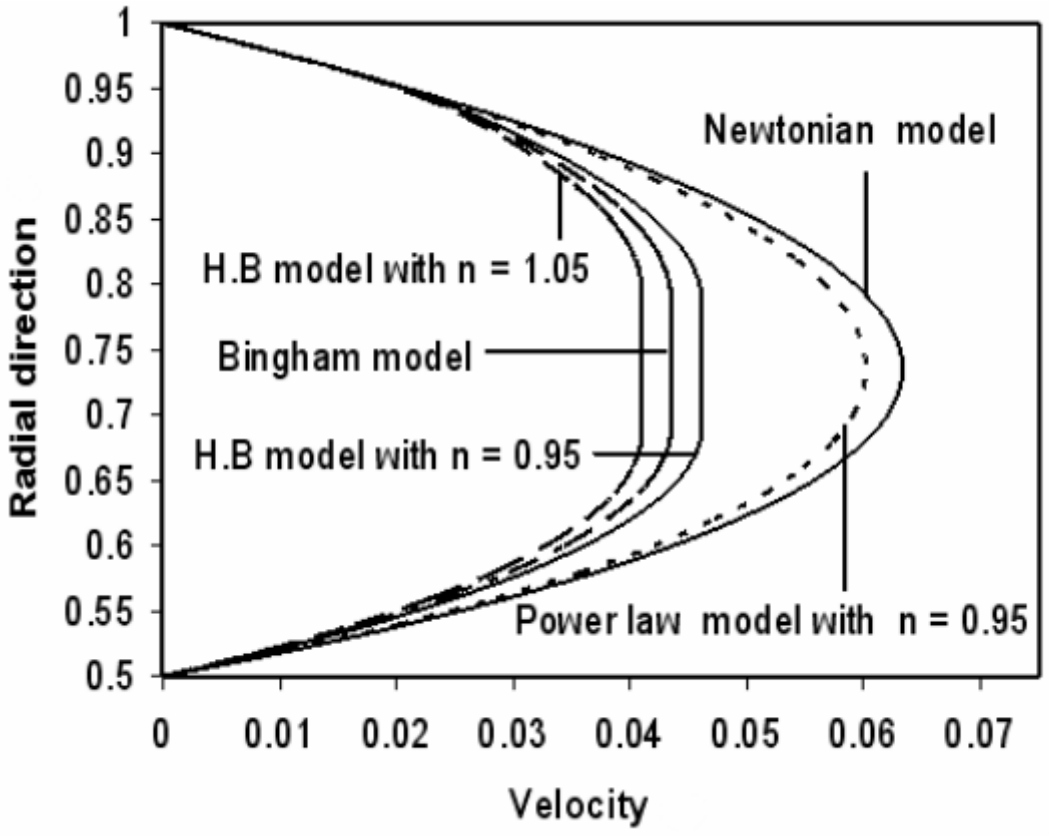

Figure 2.8: Comparison of velocity- profile of two H-B fluids, a Bingham-, a Power law- and a Newtonian fluid. H-B fluids have values for n of 1.05 and n= 0.95 respectively. Adapted from [35].

2.4 Particle Image Velocimetry (PIV)

PIV is an optical method for modelling a flow. Photos taken in rapid succession are used to make a visual representation of the fluid's dynamics. This technique can be used in a wide variety of problems including dynamics of avalanches, airflow patterns around airplanes or a fluid flowing through a pipe. The setup typically consists of a camera, a light source and the fluid which is examined. A singular camera is used for a two- dimensional velocity field, whereas a stereoscopic PIV setup consists of two cameras that examines in three dimensions. Pictures are taken as the light source shed light on the particles. This gets captured by the camera, and the images are then processed [36].

2.4.1 Particle tracking through cross-correlation

Using Matlab, the PIV software called PIVlab tracks particles in the fluid and then creates a vector field based on the velocity of particles of the flow. Each picture is divided into several subsections called interrogation windows, IWs, which are partially overlapping each other (typically 50 %). The software then approximates the field by cross correlating each of the subsections. The approximation of each velocity vector is achieved by finding the peak value for cross correlation between each image. This peak value will then be the most probable displacement for that particular area. The maximum cross correlation can be calculated through discrete cross-correlation, DCC, in Equation 2.12. [37]:

$$\underset{m,n}{max}\left(\sum_{i,\,j-1}^{M} f_t\Big(i,j\Big) f_{t+\Delta t}\Big(i+m_x, j+n_y\Big)\right) \tag{2.12}$$

Where M is number of pixels in the interrogation window. m_x and n_y are the x- and y components of the displacement factor. f_t and $f_{t+\Delta t}$ are the gray- scale values at time t and $t + \Delta t$ for each of the points [37].

Even though PIVlab offers a DCC based algorithm, it is considered outdated for digital image correlation. By instead using the frequency domain through a fast Fourier transform based algorithm, PIVlab is able to solve for the velocity vectors way faster. With this method it is also possible to use the multi-pass function which significantly improves the accuracy of the analysis. Peak value of cross-correlation, and its projection to the frequency domain is illustrated in Figure 2.9.

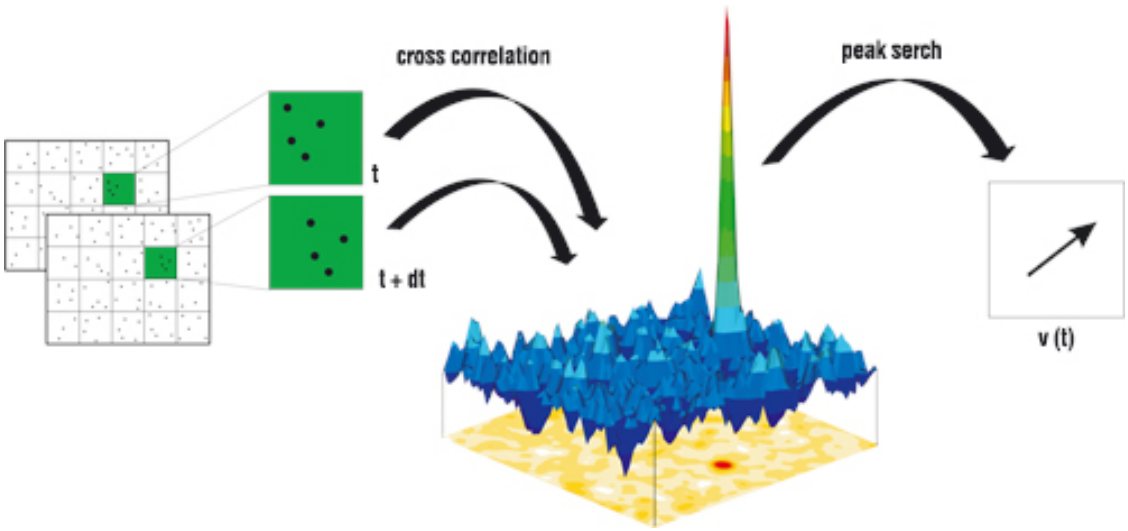

Figure 2.9: Most probable displacement and projection to frequency domain [38].

One of the biggest issues concerning the cross correlation is over- or under sizing of the interrogation window. PIVlab will miss the displacement of particles if the IW is too small, while excessive averaging is done if IW is too big. This is solved in PIVlab by using multi-pass, which is not available through the DCC algorithm. Multi-pass utilizes several sizes of interrogation windows and starts by the analysing the largest one. The first pass then works as a base for the next pass(es). [39]. The alternation of IWs are displayed in figures 2.10, 2.11 and 2.12.

Figure 2.10: Too small IW:
Displacement falls outside interrogated area [40].

Figure 2.11: Too large IW:
Many particles are treated as one [40].

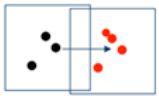

Figure 2.12: Multi-pass algorithm
A large IW acts as a base for a smaller IW [40].

Velocity v can be calculated by dividing the change in common displacement, $\Delta\overline{x}$, by the time interval between the images, Δt, as shown in Equation 2.13

$$v = \frac{\Delta\overline{x}}{\Delta t} \tag{2.13}$$

The PIV measurements will yield graphs that shows the velocity magnitude for a cross-section within the pipe. As this will be studied in two dimensions, the velocity magnitude is defined as

$$u = \sqrt{v_x^2 + v_y^2} \tag{2.14}$$

Where v_x is velocity in horizontal direction and v_y is velocity in vertical direction.

2.4.2 Theoretical procedure of PIV

Seeding particles

As the software tracks particles in the fluid, it is necessary to apply seeding particles to the liquid in order to get traceable points in a homogeneous liquid such as distilled water. When choosing tracer particles, it is important to find some that has as equal density as the investigated fluid as possible. Particles with other densities have different dynamics and will not provide an accurate representation. It is also important to not apply an excessive number of particles as they should not be a significant component of the fluid. (5-10 particles are recommended per. interrogation area for accurate results) [37].

Recording settings

When selecting time-step for each recorded picture it is important to keep in mind the velocity of the fluid. Too low framerate will result in pair loss between the interrogation areas. Before doing experiments, one should test the recording framerate by identifying PIVlab's capability of making valid vectors [41].

Light source

The most typical light source used is a laser which goes through a light sheet and then hits the particles in the flow. This must be synchronized with the camera in order to get pictures of only lit up particles. For this thesis, a LED will used which provides continuous waves of light. Hence, no synchronization will be needed.

Pre-processing

The pictures taken can be run through image pre-processing in PIVlab before being analyzed. For most experiments, the best feature here will be "enable CLAHE", which enhances the contrast.

Calibration

A calibration photo is also preferable as it translates pixels to length. It also proves more accurate than investigated photos as depth can be considered.

Vector validation and plotting

When the analysis of every photo is done, one should validate the produced vectors by selecting the region of sensible magnitude. This can be done under "vector validation" in PIVlab. The data can then be plotted to produce several profiles such as the velocity magnitude. This profile shows the common velocity through a selected cross section of the pipe and can be used to determine the fluids' velocity for a specific point.

Snell's law and PIV

If recording for PIV at an angle, through another medium, it is necessary to account for the refractive index. The difference in refractive index bends the light going through the interface of the substances and changes the appearance for the camera on the outside. Figure 2.13 illustrates the effect on light going through two substances of different refractive indexes. This thesis will study a fluid in a cylindrical pipe and must therefore take this into consideration. In a cylindrical pipe, the light will for all points except the middle be refracted in a different angle than the source emits.

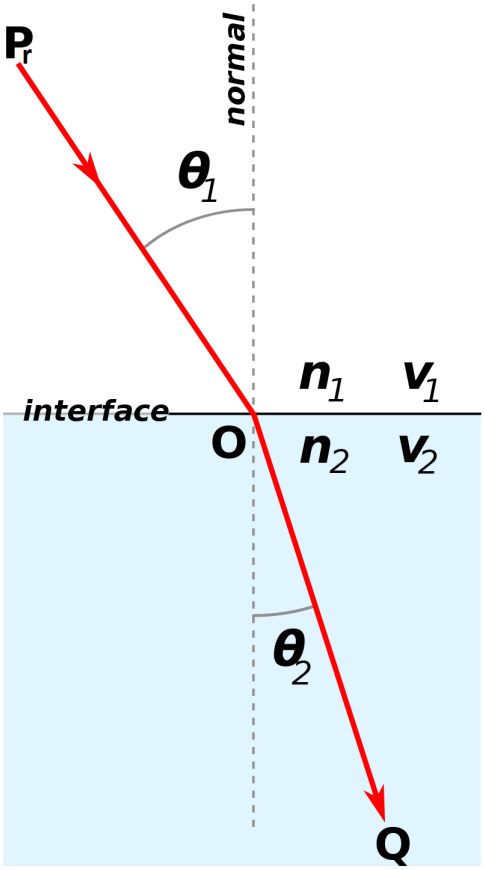

Figure 2.13: A theoretical visualization of Snell's law. Adapted from [42].

$$\frac{sin\theta_2}{sin\theta_1} = \frac{v_2}{v_1} = \frac{n_1}{n_2} \tag{2.15}$$

The two substances in Figure 2.13 have non-identical refractive indexes, $n_1 \neq n_2$. The incident ray P_r hits the interface with a different angle than the refracted ray Q, $\theta_1 \neq \theta_2$. Similarly, the velocity of the ray differs in the two substances, $v_1 \neq v_2$.

Chapter 3

Experimental work

3.1 Experimental setup

The goal of this project was to study fluids with different properties in a horizontal pipe. Therefore, the project was carried out in such a way that it would be possible to replace the fluids in the system without leaving any residue. This section will describe the general setup for the flow loop, compositions of the different fluids, procedures for the experiments, pre-sets for the rheometers and lastly digital tools utilized.

3.1.1 General setup

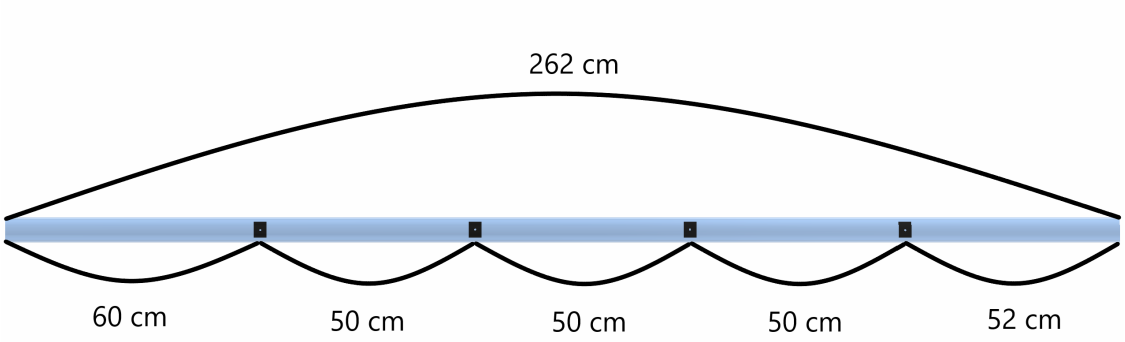

Figure 3.1: Dimensions of the pipe with PVC reinforcements.

The main component in the system is a horizontal acrylic pipe. The pipe is 262 cm long with an inner and outer diameter of 5 and 6 cm respectively. By using four smaller parts of a PVC pipe with an inner diameter of 6 cm, the pipe was reinforced. These reinforcements allowed drilling into the pipe, such that pressure taps could be installed. The PVC parts was arranged with 50 cm between each other, with the first one being placed 60 cm from the entrance. A hydrodynamic entrance length of

50 cm was calculated, so 60 cm was chosen with a safety factor of 1.2 in mind. The pipe's dimensions and PVC reinforcements are illustrated in Figure 3.1. Because of the smooth surfaces of both the PVC and the horizontal pipe, sandpaper was used to make the surfaces rougher. This would allow the adhesive to stick to both of the surfaces keeping the PVC reinforcements in place. The pipe and the reinforcements were held down by clamps for 24 hours, which was instructed on the Tec7 canister.

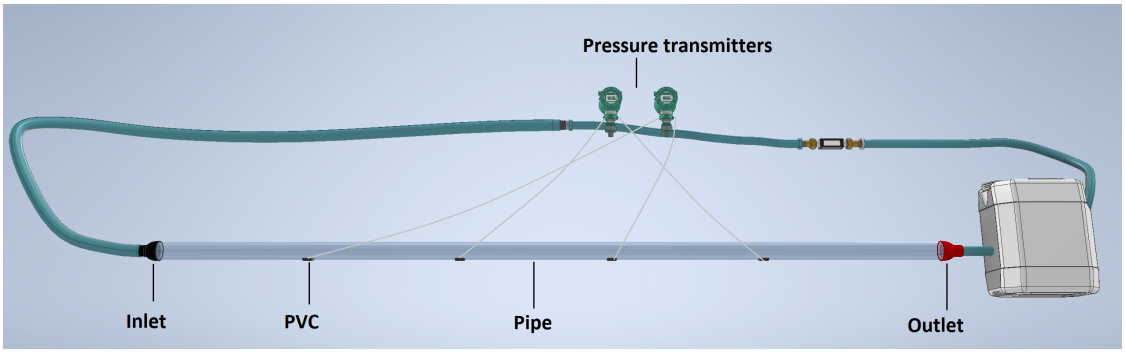

Figure 3.2: Flow loop, inlet, outlet and pressure transmitters.

A tap drill with a diameter of 3 mm was used to create a hole that penetrated both the PVC and the wall of the acrylic pipe. The hole provided the means to perform pressure measurements of the fluid flowing through the pipe. By using a tap drill with a diameter of 8.5 mm a blind hole was created with the 3 mm hole all the way through in its centre. A tapered tap was used to create threads in the larger hole, this would allow a conic fitting to create a seal by wedging the metal of the fitting to the wall of the reinforced pipe. The four fittings, or nipples, were to be connected to two pressure transmitters which was mounted atop of the tank. The transmitters were Rosemount 3051, see Figure B.10, which provided the values for the pressure differences in mbar. Originally, transmitter nr. 2 measured the pressure difference between point 1 and 2, whilst nr. 1 measured the pressure difference between point 3 and 4. This was later changed, and Figure 3.2 provides an illustration of how the tubes ultimately was set up. Transmitter nr. 1 is on the right and nr. 2 is on the left. The small tubes connecting the pipe to the pressure transmitters was in advance filled with distilled water. To get accurate measurements, the tubes had to be air-free. The water within the tubes conveys pressures up to the transmitters which in turn converts these pressure readings to an analog electrical signal [43]. The nipples were originally facing upwards, but upon filling the system with fluid, air would accumulate at the top of the pipe. This led to air entering the tubing which provided inaccurate results. This was fixed by rotating the pipe 180 degrees.

At the inlet of the pipe an aluminium honeycomb, illustrated in Figure B.12, was installed to serve as flow straightener. The honeycomb was 9 cm long and its purpose was to break up the jetstream entering the pipe. This would create a clean slate such that results from PIV measurements wouldn't be affected by the stream in the tubes leading up to the pipe. To avoid scratching the pipe because of the sharp edges on the honeycomb it was wrapped in duct tape and snuggly fit into the pipe upon

applying high vacuum grease. Both the inlet and outlet for the pipe were 3D printed. The inlet was made out of a harder material and used an O-ring to create a seal between the inlet and the pipe. The outlet was constructed from a softer material and was sealed by two tight clamp rings.

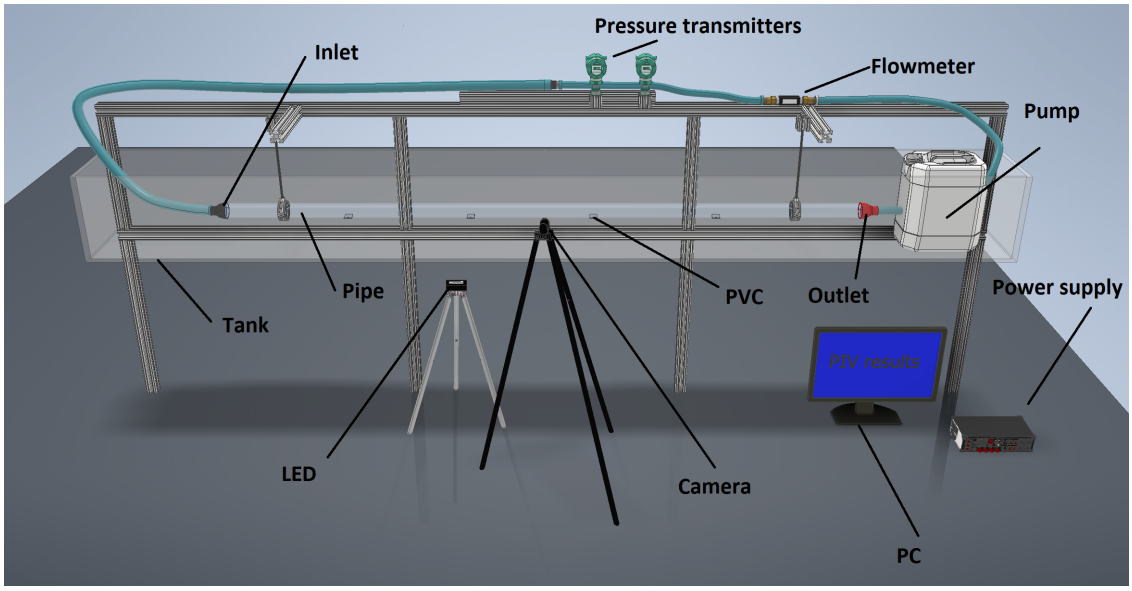

Figure 3.3: Full overview of the flow loop with all components.

Conducting Particle Image Velocimetry measurements was a central part of the project. Water and air have different refractive indexes, and if the pipe was to be studied in air, the camera would receive a slightly distorted picture because the angle of the entry ray would be different than the refracted ray. Therefore, the pipe required to be submerged in water. A large glass tank with dimension 375 × 35 × 36 cm was used. The pipe was suspended from two aluminium bars mounted on top of the tank, see Figure 3.3. The tank was filled with water until the pipe was fully submerged and was about 3 cm beneath the surface. A container was also placed within the glass tank. This container was modified so that the outlet of the pipe could be attached to its side. A larger hole was cut out at its top so that the pump that would provide flow could be installed inside. The pump was a bilge pump with the capacity of 95 L/min and is portrayed in Figure B.8. It was immersible and corrosion-resistant, which were important attributes as it would be fully submerged in fluids. The container was filled with a selected fluid such that the height of the fluid in the container, was the same as the height for the fluid in the pipe. This would prevent any pressure differences created from hydrostatic pressure in the tank, while also not pushing air back into the pipe.

The pump within the container was connected to a power supply which was used to adjust the flow rate within the system. The power supply was a Manson DC Regulated Power Supply, and was operated by a single knob which adjusted the electrical power supplied, see Figure B.9. 0.7 V was the lowest selectable voltage the power supply would provide. The pump was connected to a tube which led

into an ultrasonic flowmeter from Cynergy[3], shown in Figure B.11. This flowmeter was able to measure flow rates between 0.5 L/min and 25 L/min. Additionally, it provided accurate and non-invasive measurements [44]. The flowmeter was placed with a hydrostatic entrance length in mind as well. The inner diameter of the tube from the pump to the flowmeter was 2.5 cm, and the length was 130 cm. This equals to a length of $52 \times ID$, which is more than sufficient. Following the flowmeter was another tube that connected to the pipe's inlet, completing the loop.

Setting up the Particle Image Velocimetry had to be done with extreme precision in order to make the camera capture clear pictures of the particles flowing. The camera used is displayed in Figure B.16 and was a Basler Ace 510. The camera was connected to a computer using USB and displayed a black and white live feed of what the camera was capturing. The computer connection provided a wide range of options for settings on the camera. The camera was placed on a tripod facing the pipe horizontally with the focus on its centre, see Figure 3.4. Due to the importance of having the camera at the exact same position for each test, duct tape was used to stick the tripod's legs to the floor. The camera would examine the flow at the halfway mark of the pipe. The light source used when carrying out the tests was a ILA_5150 LPS v3 LED, see Figure B.17. This source was able to provide ultra-bright illumination in both continuous waves and pulsed repetition [45]. The LED was placed under the pipe, directly beneath the area of investigation, facing vertically upwards through the pipe.

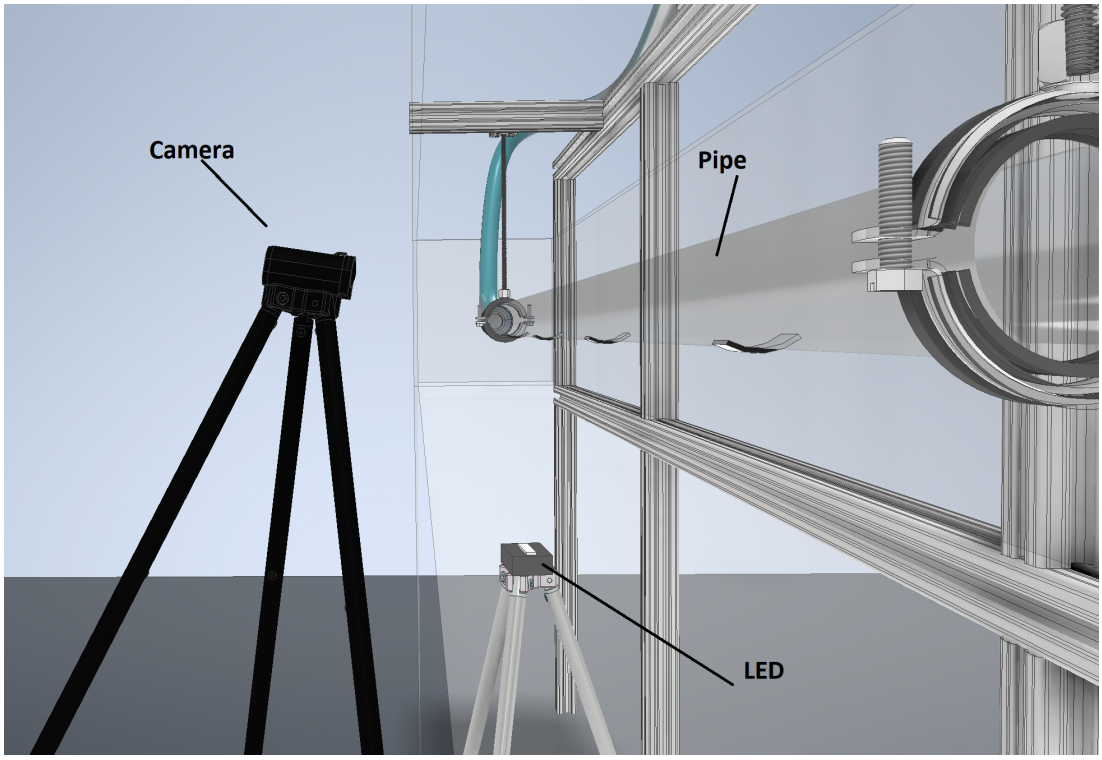

Figure 3.4: Camera and LED angled towards pipe.

When camera and LED was set up, the rest of the permanent setup was at the computer. All the recording settings was done in Pylon Viewer software. It was necessary to get the recordings saved as pictures. Therefore, the output format was changed from the standard AVI format to TIFF. The camera was set to take 200 pictures a second, for 5 seconds. This resulted in 1000 pictures that would be analysed in PIVlab, which would compose a velocity profile for the fluid inside the pipe. Recording image was also cropped to only include the part of the pipe that was of interest. Gain and gamma settings were lastly adjusted until a clear image was obtained. It was crucial that each individual picture, and every test had the same exact prerequisites.

3.1.2 Description of fluids

This project studies the characteristics of three Carbopol Ultrez 10 solutions in water. The Carbopol used is portrayed in Figure B.1. The chosen concentrations were 0.6 g/L, 0.8 g/L and 1.0 g/L. These concentrations were not chosen fully at random. Preparation reading of previous articles showed that 0.8 g/L was a typical concentration used for a viscoplastic fluid. Therefore, having concentrations slightly lower and higher as well could yield interesting results. The mixtures would consist of Carbopol, distilled water and NaOH. The NaOH is added to neutralize the low pH of the fluid. The small amounts of Carbopol being used demanded high accuracy when weighing. A NewClassic MS weight from Mettler Toledo was used and provided readability of 0.1 mg. The fluids were tested rheologically by a V-G viscometer before the project were carried to the system. The Carbopol was mixed with the distilled water using a Silverson L4RT-A mixer, which is able to mix with shear rates up to 8000 rpm. Figure B.2, B.5 and B.4 provides illustrations for the weight, the viscometer and the mixer respectively. Carbopol will upon mixing, because of its low density, float. It will also struggle to fully disperse and instead form agglomerates. These problems can be overcome using a Silverson mixer to disperse the Carbopol [46].

3.2 Experimental procedures

This section will describe in depth how the different experiments were carried out. It will provide information about test samples of Carbopol solutions, pressure tests, PIV tests, V-G meter and MCR 302 measurements. The MCR 302 is portrayed in Figure B.6. The section also includes some problems that occurred along the way, and how they were solved.

3.2.1 Sample mixing and preparation

After settling on the three different concentrations of Carbopol solutions, three samples were mixed with the intention of studying their rheology. This would provide an insight of the properties for the fluids the flow loop would be filled with. The three samples consisted of 1 litre distilled water, Carbopol polymer and 5 % NaOH. The samples were mixed for 2 minutes at 2000 RPM while adding the Carbopol. This was followed up by 10 minutes of mixing at 5000 RPM to make sure the polymer was fully dispersed. The pH for the samples were measured using a Mettler Toledo Five Easy, see Figure B.3, and an adequate amount of 5 % NaOH was added to the mixtures such that the pH value would lay between 6 and 7. Table 3.1 displays the amount of NaOH and the resulting pH.

Table 3.1: Composition of the three samples

Carbopol [g]	**Distilled water** [L]	**5% NaOH** [mL]	**Resulting pH**
0.6	1	3.5	6.60
0.8	1	5.0	6.60
1.0	1	6.5	6.63

The rheology of the samples was studied using a V-G meter. Each sample was measured three times using an increasing and decreasing RPM ramp, going from 0 to 600 RPM. They were performed both ways to study any potential rheological hysteresis. Dial readings, θ, were noted for 600, 300, 200, 100, 60, 30 and 6 revolutions per minute. The fluids were given approximately 10 seconds at each RPM in between the readings to ensure the fluid had reached equilibrium.

3.2.2 Water tests and calibration

After collecting data from the different samples, the flow loop was filled with distilled water. Various tests would be run for water including pressure test, PIV measurement and finding a correlation between the flow rate and the power supply voltage. In order to get a traceable flow within the water filled system, 28 mL of seeding particles, or tracers, were added to the water. The seeding particles are displayed in Figure B.14. A lot of air bubbles accumulated upon initially filling the system with water. The air accumulation was removed by sudden bursts of high voltage, which gradually moved them through the loop. If they were stuck in tubes, evening out sharp turns seemed to provide an easier flow path. In order to avoid leakage, the adhesive CT1 was applied. This was a permanent fix and prevented the inlet from being able to be removed. When the system was fully sealed and air-free, a selection of arbitrary values for the power supply were chosen to perform pressure measurements. The test was run from the lowest value, to the highest, and back down to the lowest. Each interval was measured for 60 seconds using LabVIEW software. When increasing/decreasing the values, 120 seconds was given to make sure the system reached a steady state before performing the next measurement. The different values selected was 1.0 V, 2.1 V, 4.7 V, 9.0 V and 11.1 V. In addition to the pressure transmitters logging data, the flowmeter was also active. Each value run on the power supply represented a value provided by the flowmeter. This test yielded a relationship between volt, flow and pressure differences in the pipe, and is presented in section 4.2.

By looking at the pressure differences in the pipe supplied by the transmitters, it became evident that transmitter nr. 2 was not working properly, although it was new, as it displayed non-logical values. Instead of only measuring the pressure difference in the interval between the third and fourth measuring point, the tubes between the nipples and pressure transmitters were rearranged. This allowed transmitter nr. 1 to measure a more central part of the tube by being connected to the first and third measuring point. This also led to measurement of pressure differences over a distance of 100 cm instead of the original 50 cm. This is illustrated in Figure 3.2. They were rearranged because this transmitter would occasionally display negative values at low flow rates. This could have been a result of the pipe wall not being completely penetrated, preventing an optimal path from the tube to the transmitter.

The last test performed on water was PIV. Seeding particles in the tube would float and stick to the wall, especially at the top of the pipe. This led to unclear pictures and poor velocity profiles. A conic pipe-brush was attached to a hose and inserted into the system to remove these particles, see Figure B.13. This would be done before the pictures were taken. After pulling out the hose, turning off the lights and waiting about 30 seconds to make sure the system is in a steady state following the insertion of the hose, the PIV measurement was carried out. The lights were turned off in the room so that the reflective particles became more prominent, making them easier to trace.

3.2.3 Viscoplastic fluid mixing and testing

Following the water tests, an amount of 16.5 L of fluid was calculated to be sufficient to fill the system. The viscoplastic fluids were mixed a day before being studied in the flow loop. They were mixed in two 10 L buckets and would use the same proportions for the components as the samples previously mixed. These batches were mixed for an extended period of time, at higher RPM because of the larger volume being mixed. They were mixed for 3 minutes while adding the Carbopol at 4000 RPM. This was followed up by 10 minutes of mixing at 6000 RPM. An adequate amount of NaOH was added to ensure the pH was between 6 and 7 and was subsequently mixed for another 10 minutes at 6000 RPM. The batches were set over night in a dark room with a lid over them. To prevent gel affecting results, the batches was mixed at 4000 RPM for 1 minute first thing the following day.

After 16.5 L of viscoplastic fluid had been poured into the system, a small sample was extracted, and its rheological properties was studied using an MCR 302 rheometer. The MCR 302 would perform a rotational test on the fluid and study its behaviour. [4] describes the test in great detail. The rotational test could be carried out by a controlled shear rate, CSR, or controlled shear stress, CSS. The CSS preset is the "classical" way of measuring yield point for a gel or a dispersion. The preset selected for this experiment was CSR, as this is similar to the procedure of the measurements performed by the V-G meter. A small plastic pipette was used to apply approximately 0.57 mL viscoplastic fluid on the MCR 302. The cone-plate displayed in Figure B.7 was attached to the apparatus to carry out the measurements. Figure 3.5 shows the setup for this plate, where the fluid is placed in between the cone-plate and the surface.

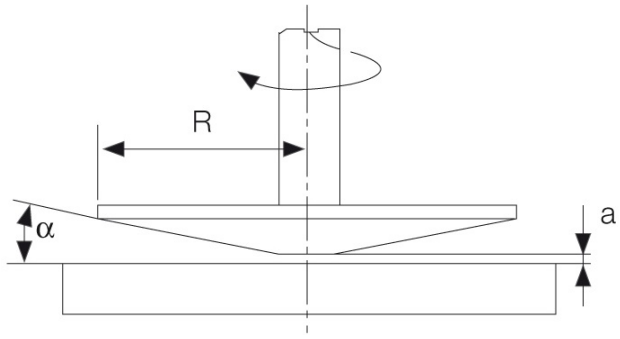

Figure 3.5: Cone-plate setup for MCR 302 [47].

In this case R is 25 mm, α is 1 degree, and a is 0.096 mm. Firstly a zero-gap procedure was performed. Because of possible thermal expansion or contraction, zero-gap tests are performed to calibrate the system. Before each measurement, the rheometer was programmed to heat or cool down the fluid to 20 degrees Celsius. When the temperature was achieved the rheometer would wait 10 minutes, giving the fluid and its polymers time to rest. Following this the fluid was rotated for 10 seconds at 10 rad/s. This would ensure that every fluid had the same prerequisites.

The viscoplastic fluids in the flow loop would undergo polymer degradation, which would alter its structures slightly. Another rheological test would therefore be carried out immediately after the measurements performed in the flow loop to give an accurate representation of the properties for the fluid in the system. Since the viscoplastic fluids were more viscous than the water, the power supply had to supply more electric power to obtain the same flow rate. To figure out the necessary volt emitted, the flowmeter would log data simultaneously as the power supply would be adjusted. The value for the flow was projected live in LabVIEW and made the calibration effortless. The pipe-brush was inserted into the tube before the PIV to get rid of accumulation of air bubbles. After it was extracted, the lights were turned off, the system was given 30 seconds to fully stabilize, and the PIV test was carried out. Contrary to water, seeding particles was not required for the viscoplastic fluids because of small air bubbles that were entrapped inside them. These bubbles served hard to remove. However, upon shedding light provided by the LED, the bubbles lit up, making them traceable.

3.2.4 Experimental procedure PIV

To begin with, tap water was filled into the glass cage to counteract the effects of different refraction indexes. While filling, a thermometer was used to keep the temperature at approximately 20 °C. Water was filled until the pipe was submerged approximately 3 cm beneath the surface. The investigated fluid was then filled into the reservoir tank, and the pump was turned on in order to fill the system with 16.5 L of viscoplastic fluid.

A thin aluminium rod with two electrical tape markings with 20 mm of space between was used to quantify the length of pictures for PIV. Measurement of the tape-gap is provided in Figure B.15. The rod was then carefully inserted into the pipe. To get a good representation of the flow through a cross section of the pipe the rod was placed as centrally as possible, as shown in Figure 3.6.

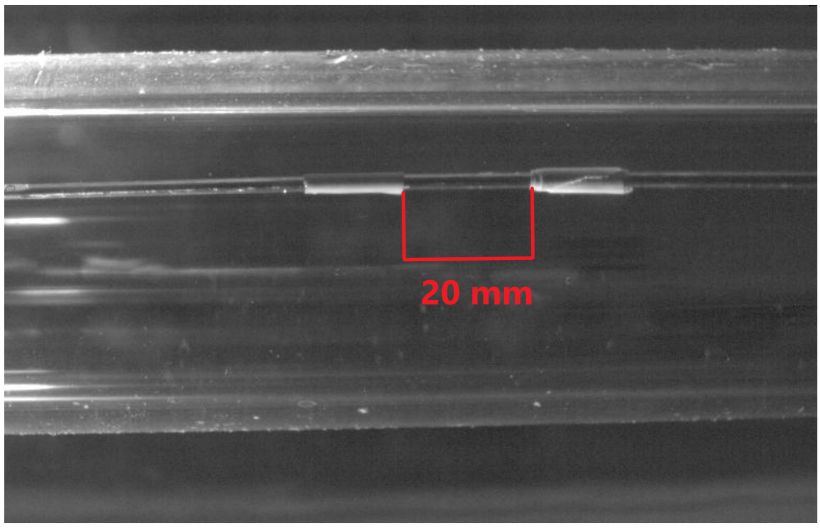

Figure 3.6: Calibration picture with tape markings on aluminium rod.

The flow rate was measured while adjusting the voltage of the pump so that the desired flow could be reached. Following this, the conic-brush was used to remove air bubbles. The flow loop was given approximately 60 seconds to reach an assumed steady state while the flow rate was monitored and recorded. The lights were then turned off, and 1000 pictures were taken over the time span of 5 seconds.

For the solution of 1 g/L the high viscosity made removal of air bubbles in the top of the pipe particularly challenging. Several attempts had to be made for usable recordings. The multiple reattempts resulted in 1.0 g/L flowing through the flow loop significantly longer than the other solutions.

3.2.5 Pressure tests and flow measurements for the viscoplastic fluids

The pressure tests for viscoplastic fluids were carried out in a different order than for water. The measurements were performed immediately after the PIV tests, which would provide information for the fluid's flow rate, provided by the flowmeter. Additionally, it would yield the pressure differences measured by transmitter nr. 1. As opposed to water, the viscoplastic fluids' properties would change over time in the system due to polymer degradation. Therefore, a single measurement describing it's behaviour wasn't sufficient. Every PIV test carried out had a corresponding pressure measurement that lasted 60 seconds.

Chapter 4

Results and discussions

This chapter will address the results obtained from the various measurements. They will be examined, explained and discussed.

4.1 Rheological characterization

The rheology of the viscoplastic fluids were studies using two different rheometers. Additionally, PIV measurements were carried out. This section will on the basis of these test, characterize the fluids by defining yield points and provide corresponding velocity profiles.

4.1.1 Results V-G meter

The V-G meter was used to conduct measurements for each of the three concentrations; 0.6 g/L, 0.8 g/L and 1.0 g/L. In this section the result for each test will be presented both individually and in a combined plot for comparison. A Herschel-Bulkley model based on the data obtained will also be presented. Further comparison between the test results can be found under subsection 4.1.3 where they are compared to the results from the MCR 302.

Execution of the Herchel-Bulkley model using least square method

The least square method was used to fit the Herschel-Bulkley model to the measured data. The procedure for this method is described below.

- In excel, each of the three parameters τ_y, n and k were given provisional values.

- The parameters were combined in the H-B equation, which yielded shear stress values.

- The squared difference between each measured shear stress and calculated, using H-B equation, where then summed up.

• Lastly the Solver Add-in in excel was used. The solver made it possible to find an exceptionally good approximation for a curve that suited the data points. It works by adjusting the three parameters until the sum of the squared differences was as close to zero as possible.

0.6 g/L Carbopol V-G meter results

Figure 4.1 displays the data obtained from examining 0.6 g/L in the V-G meter. Values for shear stress and shear rate were inserted into the Herschel-Bulkley equation using the least square method previously described. This resulted in values for yield point, consistency factor and flow behaviour index which is displayed in Table 4.1. The temperature of the fluids was measured to be 20.5 °C.

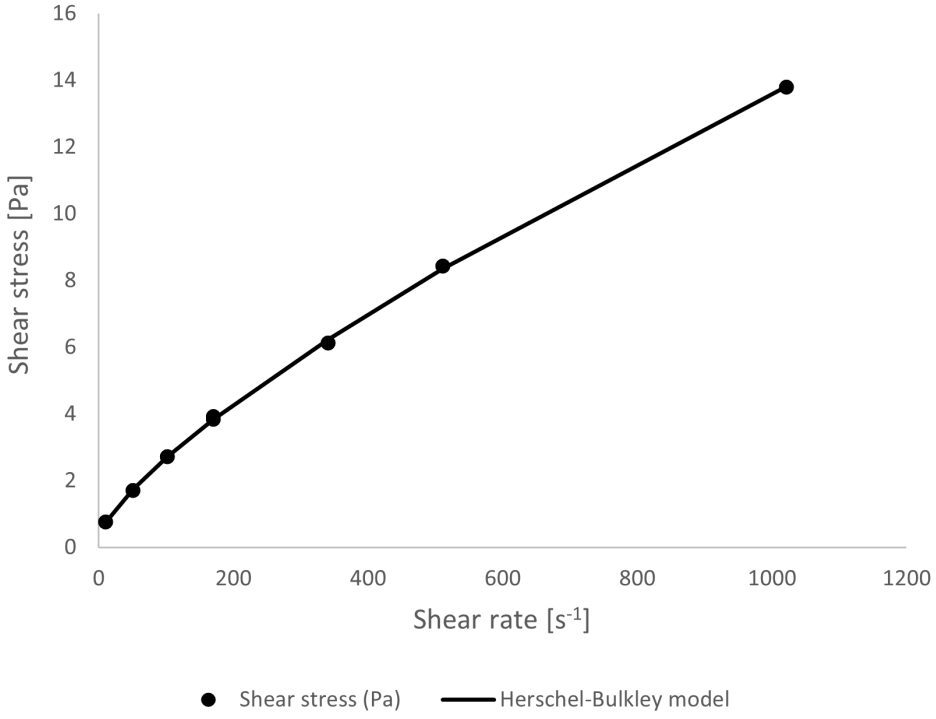

Figure 4.1: Shear rate vs shear stress for 0.6 g/L.

Table 4.1: H-B parameters V-G meter 0.6 g/L.

τ_y	0.31823192 $[Pa]$
k	0.07450247 $[Pa \times s^n]$
n	0.75037408

0.8 g/L Carbopol V-G meter results

The same procedure was done for the concentration of 0.8 g/L. This provided similar results to the previous sample, although the properties were enhanced, as shown in Figure 4.2. Table 4.2 provides the values obtained from H-B approximation. This fluid's temperature was measured to be 22.0 °C

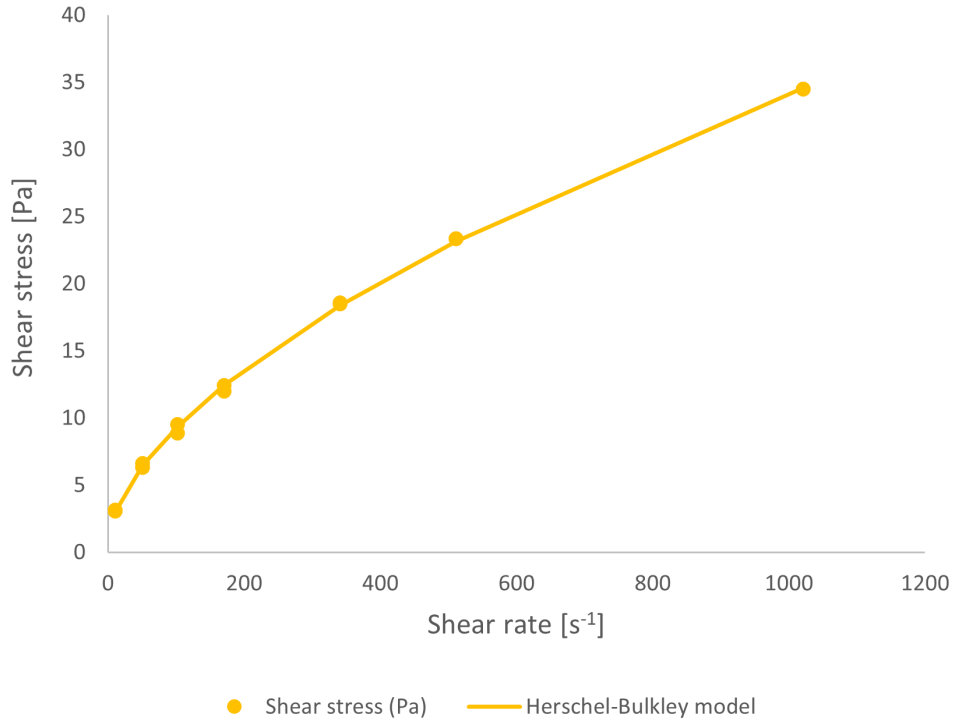

Figure 4.2: Shear stress vs shear rate for 0.8 g/L.

Table 4.2: H-B parameters V-G meter 0.8 g/L.

τ_y	0.83886253 $[Pa]$
k	0.53735421 $[Pa \times s^n]$
n	0.59756549

1.0 g/L Carbopol V-G meter results

As for the concentration of 1.0 g/L two measurements were carried out. The first was measured similarly to the others, while the second measurements was a day later. The results from the first day are displayed in Figure 4.3 and results from the other test can be found in A.0.1. H-B was used to get an approximation for how the fluid behaved between the data points. The values for this graph are provided in Table 4.3. For this test the temperature was 21.3 °C

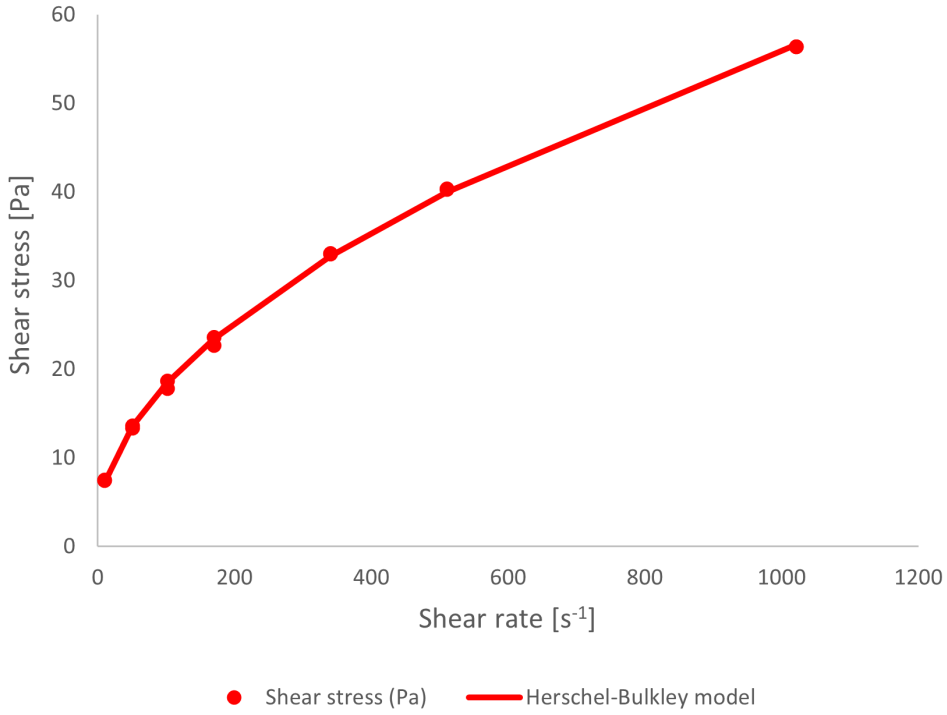

Figure 4.3: Shear rate vs shear stress for 1.0 g/L.

Table 4.3: H-B parameters V-G meter 1.0 g/L.

τ_y	2.54883609 $[Pa]$
k	1.36757825 $[Pa \times s^n]$
n	0.53065234

4.1.2 Discussion of results from V-G meter

As expected, the test results suggested a shear thinning fluid with a yield stress. Figure 4.4 shows the approximations for the data points for all three fluids.

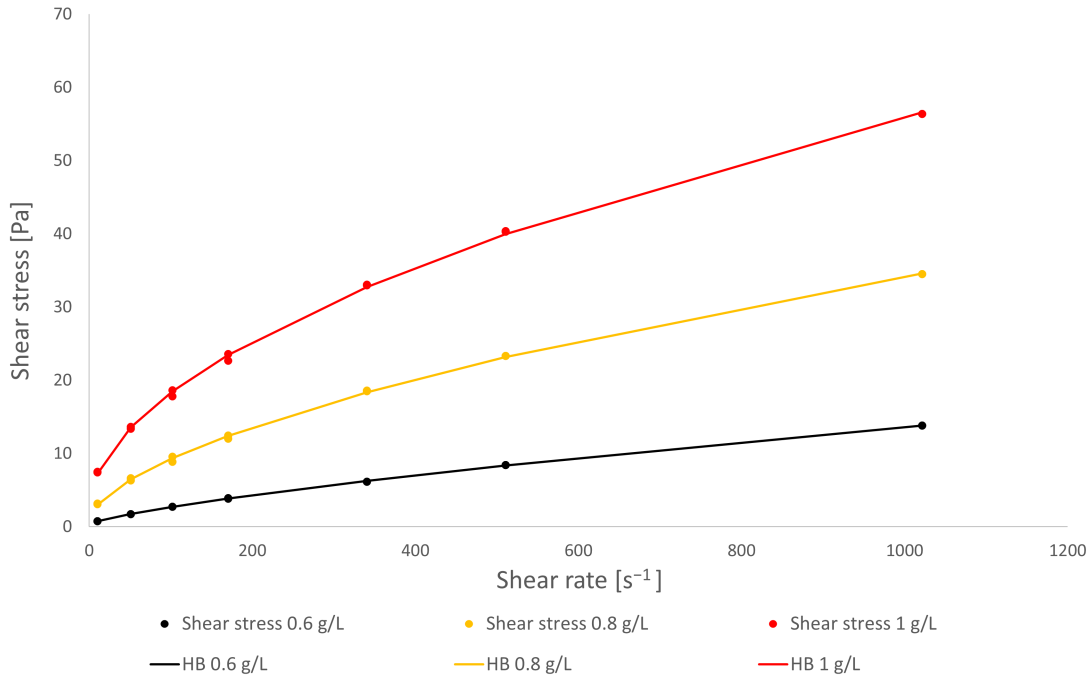

Figure 4.4: Combined V-G meter results for all concentrations.

Values for shear stress are initially increasing rapidly at low RPM, but the derivative is slowly decreasing as shear rate increases. Generally, both yield stress and shear stress increase with higher concentrations of Carbopol. The graphs also show that higher concentrations correlates to a larger shear thinning effect. Because of the steep increase at lower shear rates, it is within reason to presume the graphs will decrease accordingly with even lower shear rates. However, the limitations of the V-G meter prevent further examination.

On the V-G meter the regulation of temperature was found difficult as the tests were executed on the same day as they were mixed. This caused non-identical temperature measurements for each sample. The temperature deviation occurred due to friction while mixing.

By comparing the values provided by Table 4.1, Table 4.2 and Table 4.3 the yield stress increases with 263.6 % from 0.6 to 0.8 g/L and 303.8 % from 0.8 to 1.0 g/L.

The main goal of this experiment was to do an initial rheological investigation of the different concentrations. It was decided that the values for yield- and shear stress were sensible, and a settlement for the three concentrations were made.

4.1.3 Results from Anton Paar MCR 302 meter

The data points obtained from the MCR 302 will be presented both in the form of a Herschel-Bulkley approximation, and in a log-log plot. The Herschel-Bulkley curve shows a theoretical fitting of the curve, whilst the log-log plot makes it easier to distinguish the yield points of the fluids. The rheology was studied before and after measurements performed in the flow loop.

Figure 4.5, Figure 4.6 and Figure 4.7 illustrates the H-B approximations for the data points of 0.6 g/L, 0.8 g/L and 1.0 g/L respectively. The same procedure as for the fitting of H-B for the V-G meter was used here, including least square method. There is a total of 30 data points for each measurement from the MCR 302. 15 measurements were made when ramping up the shear rate, and 15 on the way back down.

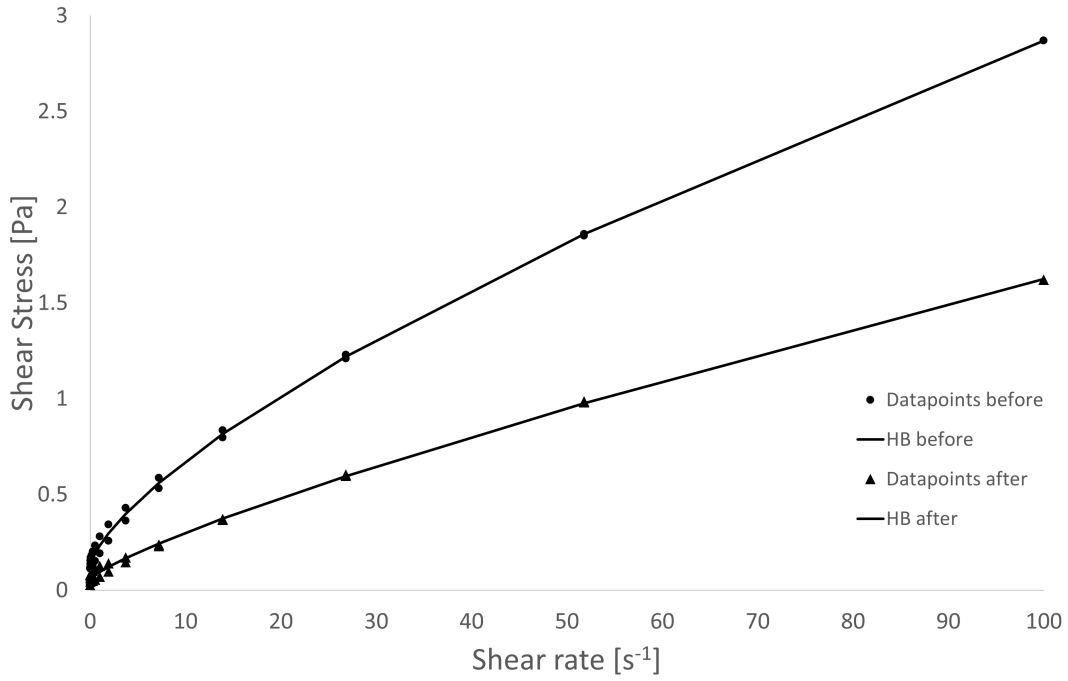

Figure 4.5: Relationship between shear rate and shear stress for 0.6 g/L before and after.

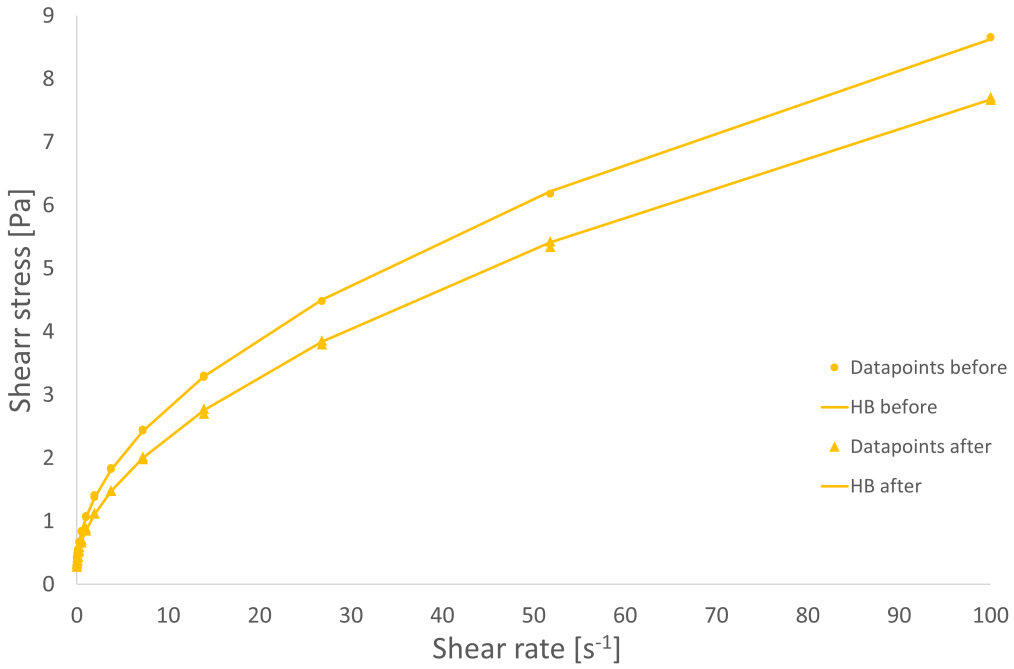

Figure 4.6: Relationship between shear rate and shear stress for 0.8 g/L before and after.

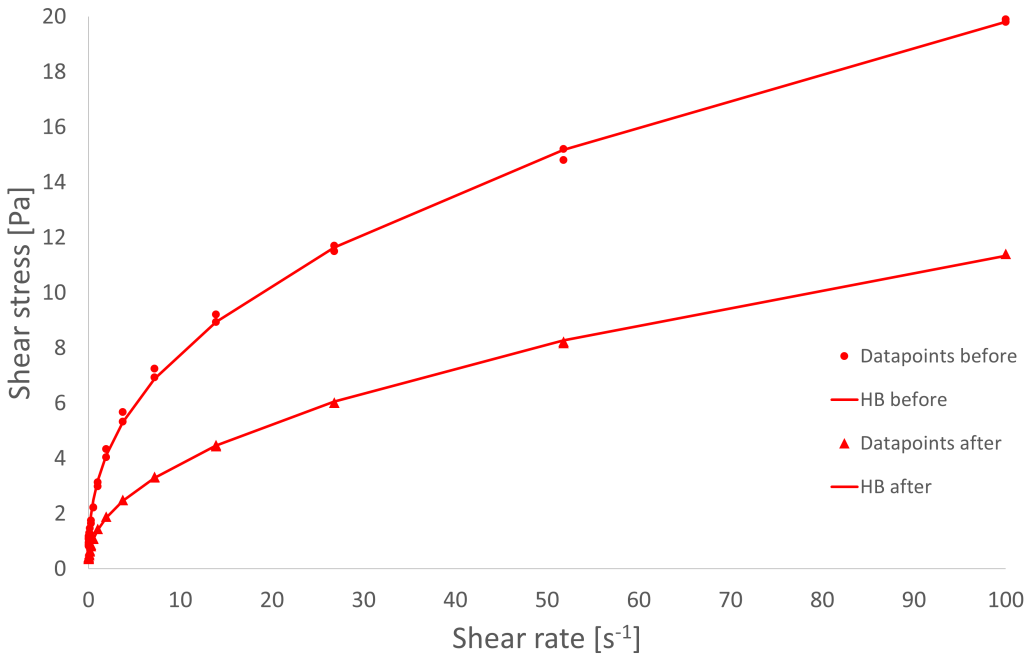

Figure 4.7: Relationship for shear rate and shear stress for 1.0 g/L before and after.

These illustrations show the relationships between shear rate and shear stress for the different concentrations of Carbopol. The dots indicate the data points obtained prior to polymer degradation for the fluid in the system, while the triangles indicate

the data points for after. Table 4.4 and Table 4.5 display the variables used in the H-B approximations.

Table 4.4: Variables of H-B approximations prior to polymer degradation.

Concentrations	$\boldsymbol{\tau_y}$ [Pa]	**k** $[Pa \times s^n]$	**n**
0.6 g/L	0.122	0.111	0.697
0.8 g/L	0.291	0.767	0.518
1.0 g/L	0.232	2.964	0.410

Table 4.5: Variables of H-B approximations after polymer degradation.

Concentrations	$\boldsymbol{\tau_y}$ [Pa]	**k** $[Pa \times s^n]$	**n**
0.6 g/L	0.058	0.037	0.813
0.8 g/L	0.277	0.575	0.554
1.0 g/L	0.234	1.167	0.489

4.1.4 Discussion of results from Anton Paar MCR 302

In order get a good representation of the proportions of the fluids properties they are all compared in Figure 4.8.

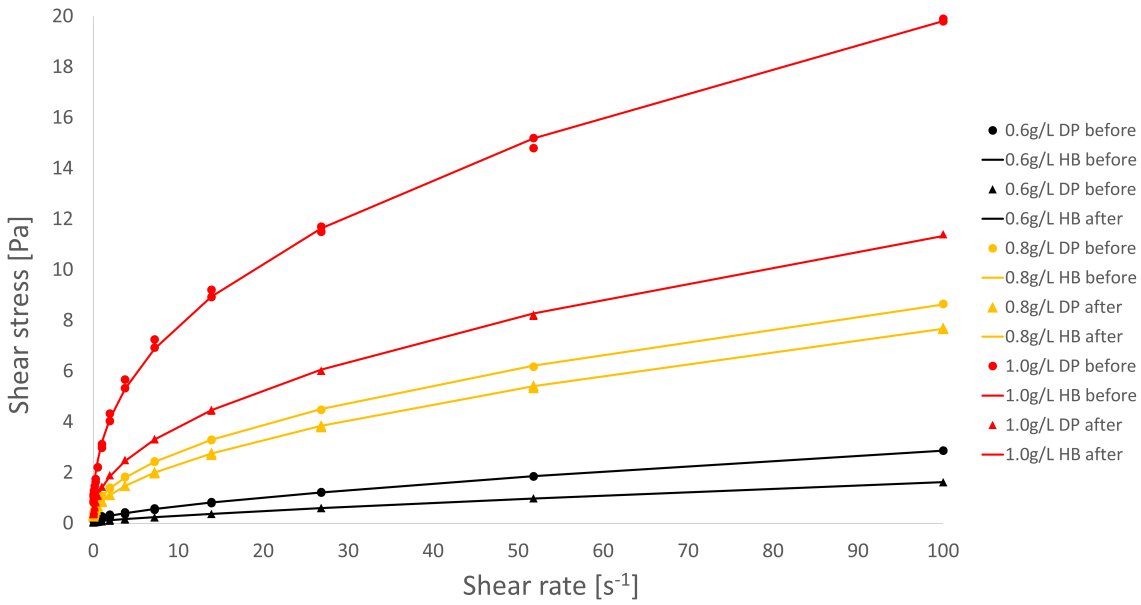

Figure 4.8: Compares all the H-B approximation from the data points.

A decrease in shear stress for each fluid after running in the flow loop is evident. The pump within the system would constantly stir the fluid, affecting the polymers. This led to a direct correlation between time spent in the system and decrease of shear stress. 1.0 g/L had the largest decrease by far, as shown in Figure 4.8. The shear stress measured at 100 s^{-1} drops by 8.4 Pa. The reason for this significant change is due to complications when performing Particle Image Velocimetry measurements, which in turn resulted in the fluid being exposed to torque from the pump for a longer duration (as mentioned in subsection 3.2.4).

Table 4.4 and Table 4.5 both describes 0.8 g/L with a higher yield stress than 1.0 g/L. The H-B approximation fails to portray an accurate representation of the yield stresses for the fluids. In order to obtain more precise values, the data points can be plotted in a log-log plot as shown in Figure 4.9.

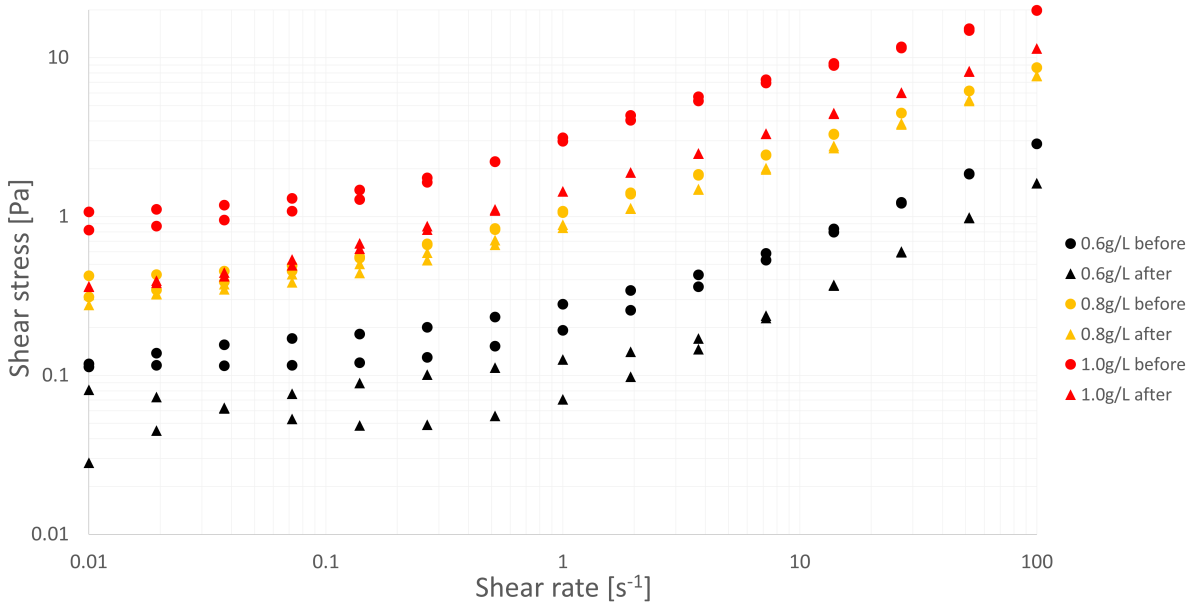

Figure 4.9: Comparison of all the data points in a log-log plot that shows the relationship between shear rate and shear stress.

By examining the shear stress values at the lowest shear rate, 0.01 s^{-1}, an approximation of the yield point can be found. As opposed to Table 4.4, this plot shows that the 1.0 g/L fluid is characterized by a higher yield initially. This is consistent with the theory since a greater concentration of Carbopol contains a higher volume fraction of solids. However, its yield following the examination in the flow loop is in the same region as 0.8 g/L's initial yield. This illustrates the significant decrease previously mentioned. By averaging the shear stresses at 0.01 shear rate, Table 4.6 provides each fluid's yield stresses prior to, and after polymer degradation.

Table 4.6: Yield stresses for each fluid based on the values from the log-log plot displayed in 4.9, before and after running the experiments in the flow loop.

Carbopol mixtures	**0.6 g/L**	**0.8 g/L**	**1.0 g/L**
Yield Stress, τ_y, initially $[Pa]$	0.116	0.368	0.946
Yield Stress, τ_y, after system $[Pa]$	0.055	0.300	0.363

By comparing the initial yield stress values to the result of the V-G meter, a significant decrease for each fluid in terms of yield stress is evident. The V-G meter characterized 0.6 g/L, 0.8 g/L and 1.0 g/L with yield stresses of 0.318 Pa, 0.839 Pa and 2.558 Pa respectively. This shows that the rheometers, though both are used to study rheology, provides significantly different values. The MCR 302 seems to provide a far better insight of the fluids at the lower shear rates. Furthermore, both rheometers require an estimation of the behaviour of the fluid for shear rates lower that they can measure. This makes the values provided by the MCR 302 more reliable.

4.2 Results from water tests

PIV- and pressure measurements were carried out on water. The PIV measurement will in this section be presented and will later on in section 4.3 be compared to the PIV results of the viscoplastic fluids. The result from the pressure test will firstly be studied, as this will give an insight of how the system works. Water served as a great template given its familiar and predictable nature.

The water pressure test conducted resulted in two graphs. Figure 4.10 displays flow as a function of volt, and figure 4.13 displays ΔP as a function of flow. As mentioned previously each point was measured for about 60 seconds, where the average flow and average ΔP being a result of that.

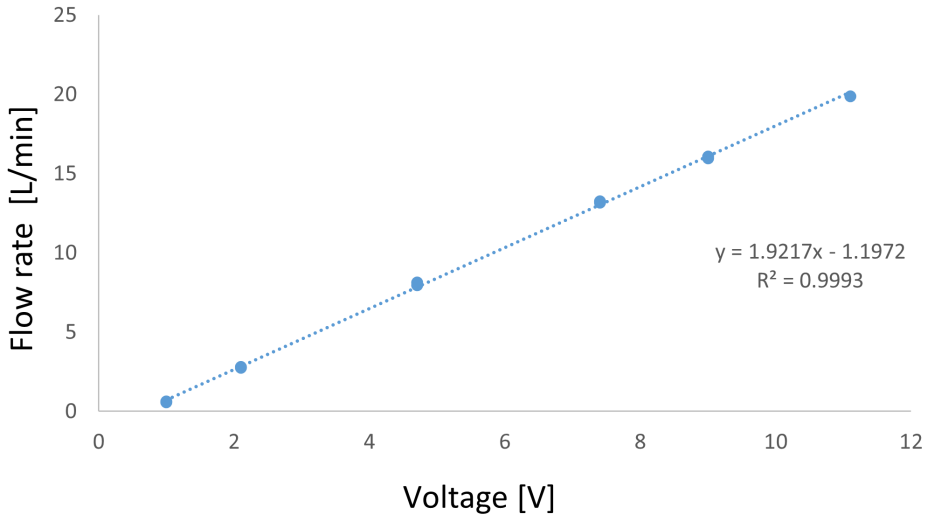

Figure 4.10: Relationship between voltage and flow rate in the system for water.

Figure 4.10 shows by interpolation a linearly increasing slope that fits the data quite well. This is also supported by the coefficient of regression R^2 being equal to 0.9993. Each data point except 11.1 V consists of 2 points. The data points in the figure appears to only consist of 1 point, indicating that there is no hysteresis present. Equation 4.1 is provided by the graph and is the correlation between volt and flow.

$$Flowrate = 1.9217 \times V - 1.1972 \tag{4.1}$$

This equation served useful when deciding a flow rate for the fluids upon carrying the PIV measurements. By taking the inaccuracies of low volt values into consideration, which will subsequently be presented, 8.5 V was chosen. This yields a flow rate of approximately 15.14 L/min and would henceforth be the desired flow rate for the PIV tests.

By extrapolating it becomes evident that the slope will cross the y-axis at a negative value. This does not make sense as there shouldn't be negative flow with 0 volt provided. The causes for this could be an offset in the flow meter, a faulty power supply or back-pressure in the system.

Back pressure would occur if the low-pressure zone, which would be located in the container, had a higher pressure than intended. This would conflict with the flow going seamlessly from left to right. The increase in pressure could be a result of hydrostatic pressure in the tank. More fluid in the tank leads to greater pressure. Another explanation may be that the flow is being pushed back into the pipe upon crashing into the tank wall. By examining the voltage where the graph would intercept with the x-axis, a value of 0.6223 V was provided. The lowest value the power supply was able to provide was 0.7 volts, which fits well with this value.

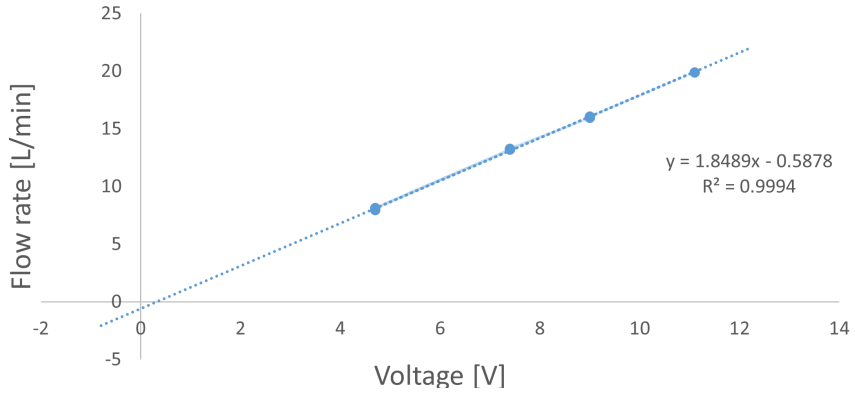

Figure 4.11: Relationship between voltage and flow by ignoring the 2 lowest values.

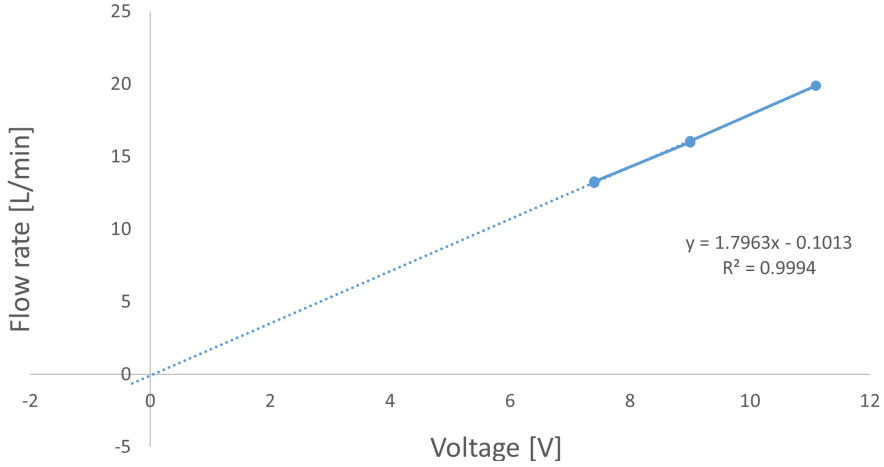

Figure 4.12: Relationship between voltage and flow by ignoring the 3 lowest values.

By examining extrapolation of the slope by removing some of the lower values, the slope will shift more towards the origin. Figure 4.11 displays the graph's change

when removing the values for 1.1 and 2.1 V. Figure 4.12 shows a graph where the values for 4.7 V are removed as well. A lot of the discrepancy could therefore be explained by the power supply becoming inaccurate when providing low values of electrical power.

The pressure differences were also logged for these flow rates. The relationship between pressure difference and flow rate for water is illustrated in Figure 4.13.

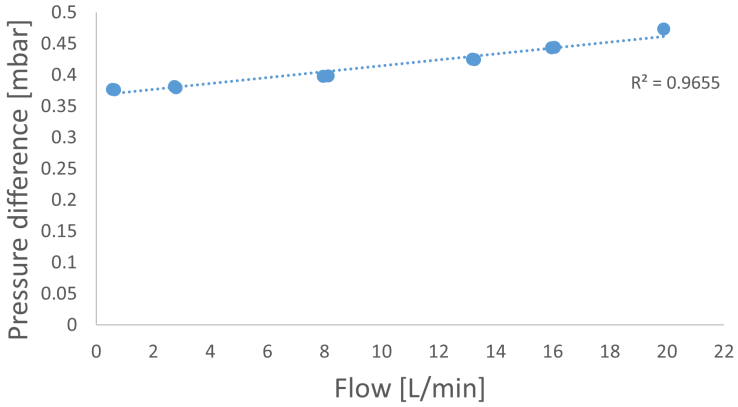

Figure 4.13: Pressure differences within the pipe as a function of flow rate for water.

Figure 4.13 displays through interpolation a linearly increasing slope that also fits the data quite well. The coefficient of regression is equal to 0.9655. The graph shows that an increase in flow leads to an increase in pressure difference between the two measuring points. The change itself is quite miniscule, being only about 0.1 mbar from the lowest to highest data point. The figure also shows that the line intercepts the y-axis at 0 flow, indicating that there exists a pressure difference between the measuring points even when the system is at rest. This should not be the case, the reason for this error could be an offset within the transmitter. It might not have been correctly calibrated, and the line should start at the origin and have the same slope as the figure from there on.

4.3 PIV results

Results from PIV and the corresponding pressure measurements will in this section be presented and discussed. Yield point is an important factor for determining the shape of the velocity profiles for viscoplastic fluids. Hence, the different profiles will be referred to as τ_1, τ_2 and τ_3.

Images from the flow recordings were transferred to PIVlab toolbox. Each processing included all the 1000 frames taken for each concentration. According to [48], arbitrary sizes of IWs could be used with FFT correlation. The interrogation area was set to 80 pixels for the first pass. The following passes were then reduced by 50 % from one to the next; $80 \rightarrow 40 \rightarrow 20 \rightarrow 10$. The pictures were then analysed, and the velocity vectors were created. Wrongly measured vectors were then filtered out through velocity-based validation in the post-processing tab.

The polyline was then drawn. This is the line that will be investigated for the velocity profiles. Therefore, this line had to be at the exact same coordinates for each of the concentrations. By running a few analyses, it was found that a vertical line through the pipe at a x-value 208 pixels would give the best results. The coordinates for this line were then saved for all upcoming tests.

The plotted data for the velocity profile of each test was then saved as an ASCII file in order to transfer it over to Excel. Results were plotted together as shown in Figure 4.14

Full velocity profile

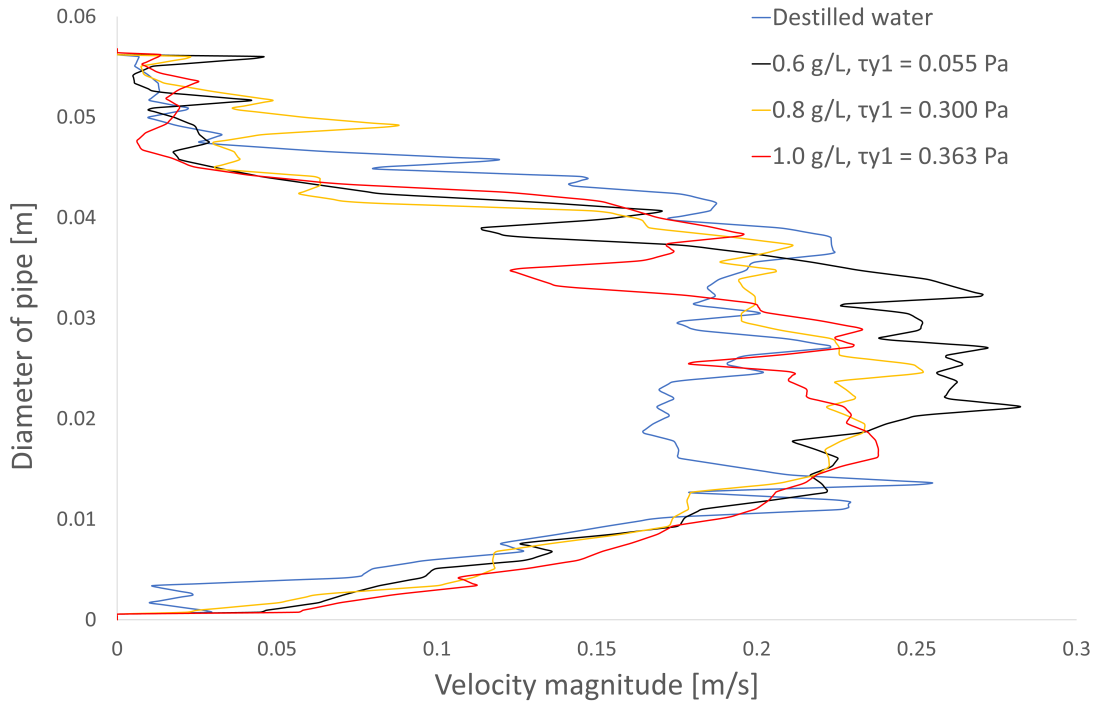

Figure 4.14: Velocity profiles of distilled water, and Carbopol concentrations of 0.6 g/L, 0.8 g/L and 1.0 g/L combined.

A polynomial could be approximated for the velocity magnitude profile in excel. The highest degree possible of six was used. This gave the R^2 values of 0.932 for water, 0.9679 for τ_1, 0.9435 for τ_2 and 0.9266 for τ_3. By applying the approximation, a simplified graph was obtained which was easier to interpret. This is shown in Figure 4.15.

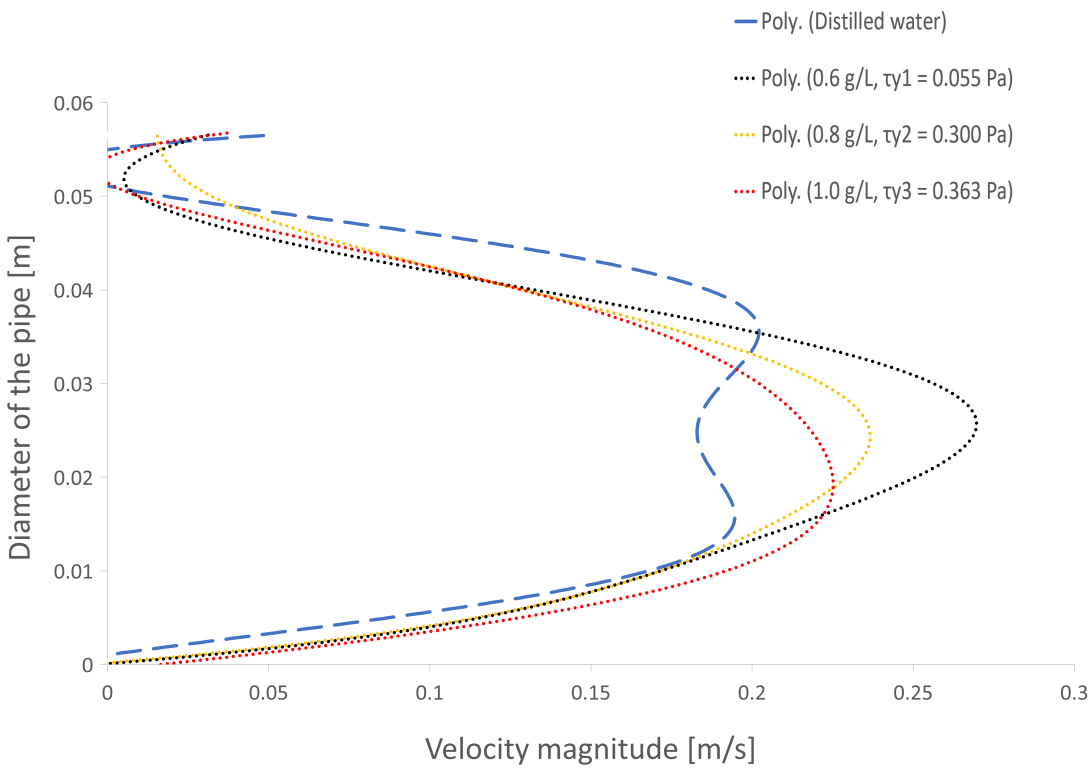

Figure 4.15: Velocity profiles of distilled water, and Carbopol concentrations of 0.6 g/L, 0.8 g/L and 1.0 g/L combined as sixth degree polynomial.

Resulting polynomial functions were as followed:

Distilled water:

$$y = 10^9x^6 - 2 \times 10^8x^5 + 10^7x^4 - 273480x^3 + 1875.8x^2 + 17.465x - 0.0193$$

τ_1:

$$y = -5 \times 10^8x^6 + 10^8x^5 - 7 \times 10^6x^4 + 222495x^3 - 3539.7x^2 + 36.797x - 0.0032$$

τ_2:

$$y = -4 \times 10^8x^6 + 7 \times 10^7x^5 - 5 \times 10^6x^4 + 165459x^3 - 3001x^2 + 35.599x - 0.0064$$

τ_3:

$$y = 3 \times 10^8x^6 - 4 \times 10^7x^5 + 2 \times 10^6x^4 - 14700x^3 - 963.89x^2 + 27.295x + 0.0165$$

4.3.1 Pressure differences and flow rates

As previously mentioned, pressure measurements were carried out for the viscoplastic fluids immediately after the PIV measurements using LabVIEW. LabVIEW logged the pressure differences for Transmitter nr. 1, as well as the flow rate provided by the flowmeter. The results from these measurements are provided in Table 4.7.

Table 4.7: Pressure differences and flowrates corresponding to PIV tests.

VP fluid	**avg.** $\Delta \mathbf{P}_1$ [mbar]	**avg. flow rate** [L/min]
0.6 g/L	0.46	15.14
0.8 g/L	2.55	15.14
1.0 g/L	5.25	15.42

Table 4.7 shows a clear correlation between an increase of pressure differences in the pipe and increase of Carbopol in the fluid. There will be more frictional forces acting in the fluid with more molecules provided by more Carbopol. Therefore, an increase of pressure loss is present. The flow rate for 1.0 g/L also deviate slightly from the two other fluids. As previously mentioned, this fluid served problematic because of rapid air accumulation. A lot of time was spent trying to get accurate results, which led to more polymer degradation. Figure 4.15 shows the velocity magnitudes for the fluids, where the flow rates from Table 4.7 characterizes them.

4.3.2 Discussion of PIV results

The PIV measurements resulted in some uninterpretable plots and made some calculations impossible. It was however still possible to see some characteristics consistent with the theory presented in chapter 2.

Possible explanation for noise

The large amount of noise prevented good comparisons between theoretical and calculated plots. It was difficult to interpret the results and find a clear pattern of the fluids' properties by increasing concentration.

Tests for both alternative sized IWs and image processions were executed without any improvement, the recordings themselves seemed to be the problem. Alternative results can be found in A.0.3. Better positioning of camera and LED, as well as refocusing of the lens could be possible solutions.

Near-wall

Irregularities at the lower values of the velocity magnitude plot in Figure 4.15 can be explained by reflections from the top of the pipe. Further discussions of the plots will therefore focus on the lower half of the plot which represents the bottom of the pipe.

Looking at the near-wall velocity magnitude in Figure 4.15, τ_3 has distinctly higher velocity gradient, $\frac{\partial u}{\partial y}$, than the other two laminar/critical Carbopol profiles. As for τ_1 and τ_2, the data collected was indistinguishable. If reliable velocity gradients were supplied, the yield points for the fluids could have been calculated using Equation 2.7.

Resulting flow profile

In Figure 4.15 the velocity profiles of the Carbopol solutions suggests a laminar to critical flow profile. As explained in section 2.1.4 this indicates that the fluids have a Reynolds numbers of less than 4000. However, for water a turbulent flow is suspected. The apparent flow profiles can be explained by the increasing Re for lower concentrations. The peak of the velocity magnitude increases, see Figure 2.5, until the critical value of $Re = 4000$ is reached and the flow becomes turbulent for water. It was in this thesis, unlike in Figure 2.5, used approximately constant flow rates. This explains the width increase for more plugged profiles. Re calculations for water can be found in section 4.3.2.

Re for water in PIV tests

By utilizing Equation 2.6, the Reynolds number for water from PIV tests can be calculated. Results for ΔP and Q in section 4.2 provides the flow rate of 15.14 L/min. This corresponds to a mean speed of approximately 0.129 m/s for a pipe of radius 2.5 cm.

The dynamic viscosity of water at 20 °C can be approximated to be $1{\times}10^{-3}$ Pa, and the density 1000 kg/m^3. Considering this:

$$Re = \frac{\rho V_{avg} D}{\mu} = 6535.96$$

Since $Re > 4000$, the suspicion of a turbulent flow profile for water is supported. For mixtures of Carbopol, the viscosity will as mentioned in section 2.1.1 be highly dependent on the shear rate and vary throughout the cross-section of the pipe. Therefore, it was not possible to calculate Re for Carbopol solutions, and the assumption of laminar to critical flow regimes were fully based on the shape of the velocity magnitude profiles.

Effect of Yield stress

As mentioned in section 2.1.4 the yield stress of a fluid running through a pipe can be calculated from the velocity profile by using Equation 2.7. Since the unyielding plug was undefinable, the calculation of yield stress was not possible. It can however be observed that by increasing the concentration of Carbopol a wider and more plugged velocity profile is present. This again suggests a higher yield point for higher concentrations.

Chapter 5

Conclusion

Successful measurements of PIV study of viscoplastic fluids in horizontal pipe have been achieved. The rheometers provided measurements of viscoplastic fluids' behaviour and was, by using H-B approximation with least square method, accurately described. Through this, yield stress values were able to be determined. The three Carbopol solutions yielded predictable and satisfactory results. Successful water measurements and comparisons were also achieved. Additionally, this reliable fluid's flow profile was even determined through PIV measurement and through calculation using Reynolds number.

The most extensive part of this project was the mechanical setup of the horizontal pipe submerged in the tank. A considerable amount of time was spent finding parts and putting the components together. Smaller hiccups such as leaking from inlet, outlet and flowmeter also served time demanding as the system could not be operated before it was completely sealed. The adhesives used took 24 hours to dry, which meant whenever they were applied, testing would be suspended by at least another day. Problems would also appear upon carrying out experiments which often times led to quick fixes. However, some problems also led to some alteration in both the procedures and results. Air bubbles from the pipe entering the tubes connected to the transmitters were fixed by simply rotating the pipe. The faulty transmitter on the other hand led to more complication. The transmitter was fully excluded, and the tubes were rearranged in such a manner that the transmitter still working studied the area of interest. In the end this transmitter alone provided sufficient data. The flow loop was constructed such that it was able to provide reproducible results, with the opportunity to swap the fluids in the future.

This thesis was purely experimental with emphasis on determining yield points for viscoplastic fluids. Various experiments and measurements was carried out where the rheology were examined using two different rheometers. Both the V-G meter and the MCR 302 provided results which characterized shear thinning yield stress fluids. However, the V-G meter resulted in higher yield point than the MCR 302. It is within reason to believe than the data provided by the MCR 302 is more accurate because of its ability to digitally measure shear stress values at far lower shear rates. Additionally, the tests carried out showed the huge effect polymer degradation had

on the properties for the fluids. The polymer degradation occurred when performing PIV-, pressure-, and flow measurements. The PIV measurements yielded somewhat unclear and distorted results, nevertheless, the data was still useable and the results were consistent with the theory. Four velocity profiles were portrayed, one of them being turbulent, and the other three laminar/critical. Aside from the faulty transmitter, the pressure measurements yielded acceptable results. The flow measurements for water yielded inconsistent results for the lower flow rates. Ideally, the ultrasonic flowmeter should have been calibrated using an electromagnetic flowmeter to figure out if the flowmeter was the cause for the deviation at low flow rates. Most likely it was due to the power supply, nevertheless, the problem was avoided by using higher consistent flow rates.

For further work it is recommended to use another power supply, calibrate flowmeter, remove air bubbles from mixtures and possibly carrying out PIV measurements on lower flow rates, such that the velocity profiles are definitely within the laminar region.

References

[1] Antoine Poumaere, M. Moyers-Gonzalez, C. Castelain, and T. Burghelea. Unsteady laminar flows of a carbopol® gel in the presence of wall slip. *Journal of Non-newtonian Fluid Mechanics*, 2014.

[2] Ian Frigaard. Simple yield stress fluids, volume 43. October 2019.

[3] S. Leimgruber I. A. Frigaard and O. Scherzer. Variational methods and maximal residual wall layers. 20 May 2003.

[4] Thomas G. Mezger. *The Rheology Handbook*. Vincentz, 3rd revised edition, 2021.

[5] A. Malkin, A. Y. Israyev. *Rheology. Concepts, Methods, and Applications*. Chemtec Publishing, 3rd edition, 2017.

[6] The editors of Anton Paar Wiki. Basics of rheology. `https://wiki.anton-paar.com/no-en/basics-of-rheology/#basics-of-rheology`, accessed: 01.05.21.

[7] The editors of Anton Paar Wiki. Figure 4.2. `https://wiki.anton-paar.com/no-en/basics-of-rheology/#data-imagegroup-18471`, accessed: 01.05.21.

[8] Engineering ToolBox. Absolute, dynamic and kinematic viscosity. `https://www.engineeringtoolbox.com/dynamic-absolute-kinematic-viscosity-d_412.html`, accessed: 07.05.21.

[9] The editors of Anton Paar Wiki. Viscosity and viscometry. `https://wiki.anton-paar.com/no-en/basic-of-viscometry/`, accessed: 01.05.21.

[10] Elert G. Viscosity. `https://physics.info/viscosity/`, accessed: 04.05.21.

[11] Universitetet i Stavanger. Øvinger i bore- og brønnvæsker, Kompendium. 19. Januar 2010.

[12] A. Fontaínhas and C. Fernandes. Injection moulding simulation using openfoam, figure 4 (text removed). January 2019.

[13] Editors of AMCO Polymers. Molecular weight and the effects on polymer properties, jan 29, 2018. `https://www.amcopolymers.com/resources/blog/molecular-weight-and-its-effects-on-polymer-properties`, accessed: 06.05.21.

[14] Comité des Techniciens. *Drilling mud and slurry rheology manual*. Springer, reprint of original 1st ed. 1982 edition, 2012.

[15] The editors of Anton Paar Wiki. Figure 1: Filamentary molecules of a polymer solution or polymer melt. https://wiki.anton-paar.com/no-en/internal-structures-of-samples-and-shear-thinning-behavior/#data-imagegroup-18540, accessed: 13.05.21.

[16] The editors of Anton Paar Wiki. Internal structures of samples and shear-thinning behavior. https://wiki.anton-paar.com/no-en/internal-structures-of-samples-and-shear-thinning-behavior/, accessed: 13.05.21.

[17] R.H. Turner Y.A. Çengel, J.M. Cimbala. *Fundamentals of thermal-fluid sciences*. Boston: McGraw-Hill Education, 3rd edition, 2017.

[18] The editors of gunt.de. Hm 150.01 pipe friction for laminar / turbulent flow. https://www.gunt.de/en/products/fluid-mechanics/steady-flow/fundamentals-of-steady-flow/pipe-friction-for-laminar-turbulent-flow/070.15001/hm150-01/glct-1:pa-148:ca-151:pr-548, accessed: 11.05.21.

[19] The Editors of Encyclopaedia Britannica. Turbulent flow, physics. https://www.britannica.com/science/turbulent-flow, accessed: 04.05.21.

[20] Ian Nesbitt and Jukes Liu. Transition to turbulence. http://wiki.geodynamics.umaine.edu/index.php/Transition_to_Turbulence, Created: 19.02.19, accessed: 04.05.21.

[21] Hua-Shu Dou. Figure 1. https://www.researchgate.net/publication/2147222_Energy_Gradient_Theory_of_Hydrodynamic_Instability, Created: 03.04.2014.

[22] The editors of oilfieldwiki.com. Plug flow. http://www.oilfieldwiki.com/wiki/Plug_flow, accessed: 01.05.21.

[23] Dhruv Mehta, Adithya Krishnan Thota Radhakrishnan, Jules van Lier and Francois Clemens. A wall boundary condition for the simulation of a turbulent non-newtonian domestic slurry in pipes. Published: 30.01.2018.

[24] Dhruv Mehta, Adithya Krishnan Thota Radhakrishnan, Jules van Lier and Francois Clemens. Figure 4. https://www.researchgate.net/publication/322800036_A_Wall_Boundary_Condition_for_the_Simulation_of_a_Turbulent_Non-Newtonian_Domestic_Slurry_in_Pipes, Published: 30.01.2018.

[25] Cimbala J. M Cengel, Y. A. *Fluid mechanics: Fundamentals and applications*. Boston: McGraw-HillHigher Education, third edition edition, 2006.

[26] Frank M. White. *Fluid Mechanics*. McGraw-Hill, 7th edition edition, 2011.

[27] Arild Saasen and Jan Ytrehus. Viscosity models for drilling fluids—herschel-bulkley parameters and their use. *Energies*, 13, 2020.

[28] Fann Instrument Company. *Model 35 Viscometer Instruction Manual*. Fann Instrument Company, January 2016.

[29] C. Lam and S. A. Jefferis. Interpretation of viscometer test results for polymer support fluids, fig. 1. direct-indicating viscometer. May 22, 2014.

[30] The editors of Anton Paar Wiki. `https://www.anton-paar.com/no-en/products/details/rheometer-mcr-102-302-502/`, accessed: 29.04.21.

[31] Rajendra P. Chhabra. *Rheology of Complex Fluids - Chapter 1, Non-Newtonian Fluids: An Introduction*. Springer Science and Business Media, 2010.

[32] The Editors of DrillingFormulas.Com. Types of flow and rheology models of drilling mud. `https://www.drillingformulas.com/types-of-flow-and-rheology-models-of-drilling-mud/`, accessed: 15.04.21.

[33] The Editors of Schlumberger Oilfield Glossary. Bingham plastic model. `https://glossary.oilfield.slb.com/en/terms/b/bingham_plastic_model`, accessed: 15.04.21.

[34] Abioye P. Oluwabunmi Folayan J. Adewale, Anawe P. Lucky and Elehinafe F. Boluwaji. Selecting the most appropriate model for rheological characterization of synthetic based drilling mud. (2017.

[35] Usik Lee D. S. Sankar. Two-fluid herschel-bulkley model for blood flow in catheterized arteries, fig. 6 (text removed). `http://www.j-mst.org/On_line/admin/files/22-02048_1008-1018_.pdf`, Accepted: 30.01.2008.

[36] Sandijs; Kozlowski Bartosz Zhang, Chen; Vasilevskis. Particle image velocimetry-user guide. (2018.

[37] Y.-C. Tai R. Martino M.N. Papa C.-Y. Kuo L. Sarno, A. Carravetta. Measuring the velocity fields of granular flows – employment of a multi-pass two-dimensional particle image velocimetry (2d-piv) approach. (Available online 31.08.2018.

[38] The editors of piv.de. Piv image evaluation. `https://www.piv.de/piv/measurement_principle/page_1.php`, accessed: 30.04.21.

[39] Klaus Regenauer-Lieb David Boutelier, Christoph Schrank. 2-d finite displacements and strain from particle imaging velocimetry (piv) analysis of tectonic analogue models with tecpiv. Published: 15.07.2019.

[40] Ken Kiger (UMD). Piv basics: Correlation. `http://www.civil.ist.utl.pt/~ruif/SUMMER_SCHOOL/presentations/PIV_basics_correlation_final.pdf`, 2015.

[41] Louise Lu and Volker Sick. High-speed particle image velocimetry near surfaces. https://www.ncbi.nlm.nih.gov/pmc/articles/PMC3728919/, accessed: 26.04.21.

[42] The editors of wikipedia.org. Snell's law (text added). https://en.wikipedia.org/wiki/Snell%27s_law, accessed: 26.04.21.

[43] The editors of sea.omega.com. Pressure Transducers. https://sea.omega.com/th/prodinfo/pressuretransducers.html.

[44] Sensata Technologies. Ultrasonic flowmeter 0.5-25 l/min. https://www.cynergy3.com/product/ultrasonic-flowmeter-05-25-lmin, accessed: 08.05.21.

[45] ila5150. LED Pulsing System PIV V3. https://www.ila5150.de/en/piv-solutions/led-pulsing-system-lps-v3, accessed: 10.05.21.

[46] The editors of Silverson.com. Dispersion and hydration of carbopol®. https://www.silverson.com/us/resource-library/application-reports/dispersion-and-hydration-of-carbopol, accessed: 22.04.21.

[47] The editors of Anton Paar Wiki. Figure 2.2: Measuring systems. https://wiki.anton-paar.com/en/basics-of-rheology/#data-imagegroup-18450-2, accessed: 11.05.21.

[48] William Thielicke. Pivlab tutorial. https://pivlab.blogspot.com/p/blog-page_19.html, accessed: 23.04.21.

Appendix A

Additional results

This appendix presents additional results from experiments and measurements. More specifically, supplementary results from the V-G meter, PIV measurements and MCR 302.

A.0.1 Additional V-G meter results and discussion

After carrying out all the experiments presented in subsection 4.1.3, an identical to the 1.0 g/L batch was stored overnight for further testing. This was because air accumulated in the form of bubbles upon mixing. Letting the fluid rest overnight could possibly lead to a decrease of air. Figure A.1 shows the difference between the two samples.

Figure A.1: Air bubble comparison. Left is original sample; right is the next day.

On day two, the sample was suspected to be characterized by gelling. To counteract gelling there needs to be applied a force great enough to break the bindings. Therefore, the sample was mixed again before another examination. Figure A.1 shows little difference in the amount of air bubbles. Air bubbles in Carbopol solution served hard to remove. The result from the measurement is displayed in Figure A.2, where the original data points for 1.0 g/L is also present.

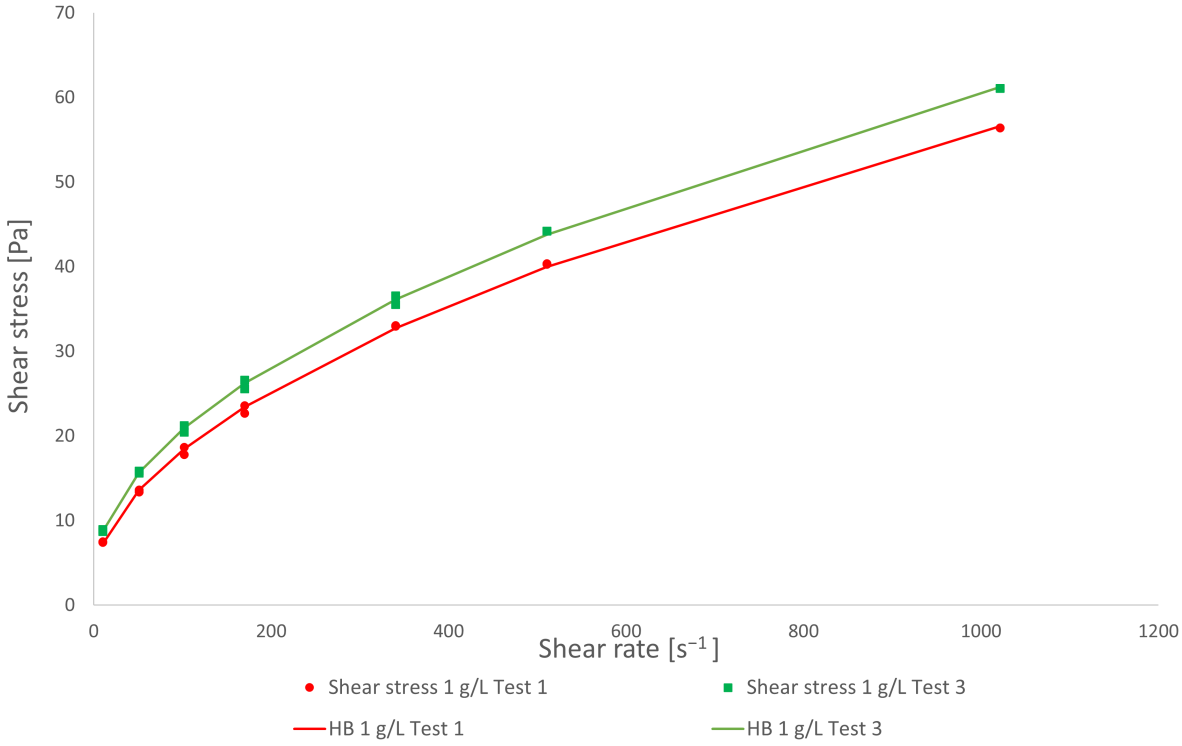

Figure A.2: Compares the results for 1 g/L.

Figure A.2 shows that the examination performed on the following day deviated noticeably from the first test. The graph was shifted upwards, displaying higher shear stress values. It has previously been shown that polymer degradation lowers the fluids shear stress in relation to shear rate. However, in this case it seems that the gelling was not completely broken down, and that it affected the fluid in a greater degree than the polymer degradation. The first fluid's temperature was measured to be 21.3 °C, the latter was 21.9 °C. Table A.1 displays the values for the variables used in the H-B approximation.

Table A.1: H-B parameters V-G meter 1.0 g/L second measurement.

τ_y	3.45129721 $[Pa]$
k	1.58565319 $[Pa \times s^n]$
n	0.51890835

Recall that the yield stress for 1 g/L was 2.54883609, see Table 4.3. By comparing that value to the yield stress values provided by Table A.1 the yield stress increases by 35.4 %. This made it clear that as similar prerequisites as possible for each test should be strived for. This big increase empathizes the importance of stirring the mixture when left over night. The temperatures will also have a direct impact on the fluids shear stress and viscosity. The temperature deviation was minor, nevertheless, it is still an important factor and should not be overlooked.

A.0.2 Additional data from rotational test MCR 302

Upon performing the examination using the Anton Paar rheometer, a lot of excessive values were provided. Most of them were discarded as they are not relevant for this thesis, however, some of them can be utilized to examine some of the key features of viscoplastic features. This subsection will study the apparent viscosity acquired from rotational tests. The difference of properties caused by stretched polymers is not of any interest in this subsection. Therefore, only the apparent viscosity of the three fluids before they were run through the flow loop are presented.

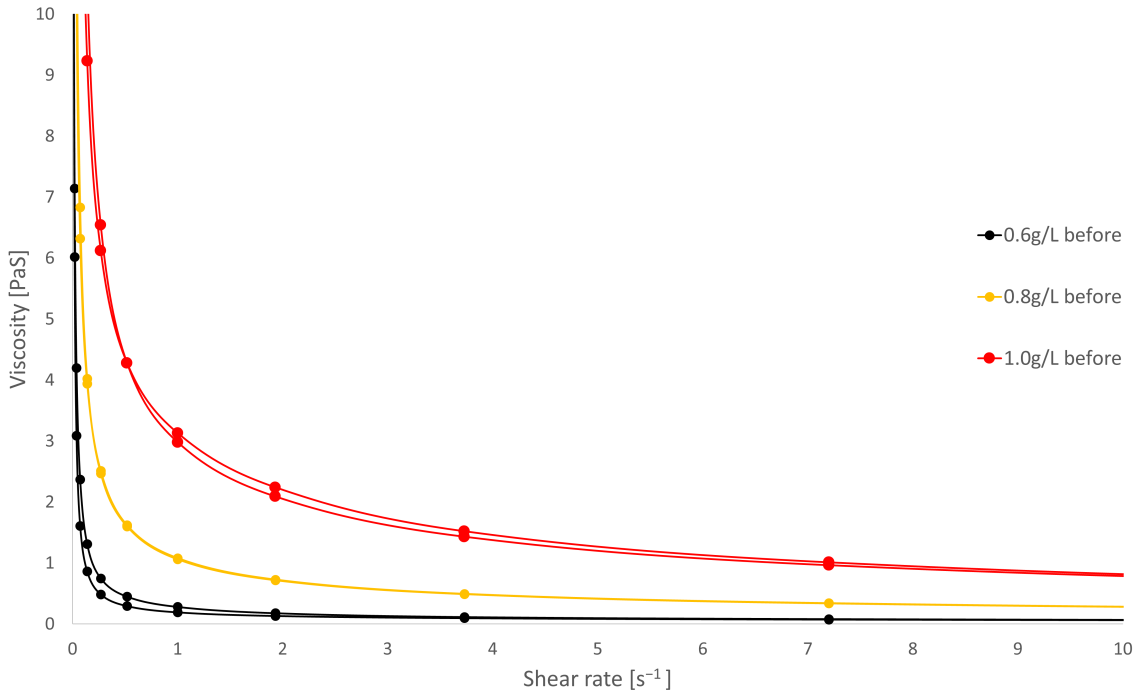

Figure A.3: Illustrates the apparent viscosity for the three VP fluids.

The axis in Figure A.3 are cropped such that viscosity goes from 0 to 10 Pas, and shear rates are shown up to 10 s^{-1}. This way, the focus is shifted towards where the graphs have a significant change of orientation, while also providing descriptions of their behavior for lower shear rates. The data points are plotted as dots, while the lines between them are theoretical. The measured data provided are obtained from the same previous increasing and decreasing shear rate ramp.

Discussion apparent viscosity

As presumed, higher concentration of Carbopol provided higher viscosity. This comes across clearly in Figure A.3 where 1.0 g/L values for viscosity lies higher than those for 0.8 g/L, the same goes for 0.8 g/L and 0.6 g/L. The viscosity changes as a function of shear rate, indicating that they are shear rate dependent, which supports the claim of them being Non-Newtonian. Additionally, all three slopes show tendencies

of shear thinning fluids, which fits the description of viscoplastic properties. The figure also shows signs of a yield stress. The viscosity for the fluids is described by a large increase when studying the lower shear rates. 0.6 g/L, 0.8 g/L and 1.0 g/L reaches values of 11.3 Pas, 31.2 Pas and 107 Pas at 0.01 s^{-1} respectively. These are not included in the graph as the proportions made them uninterpretable.

A.0.3 Alternative PIV results

Apparent noise on the velocity magnitude profiles resulted in several new analyses using alternative settings, in an attempt to purify the results. This subsection will only focus on the PIV settings and how they affect flow profiles, rather than actual values obtained from them.

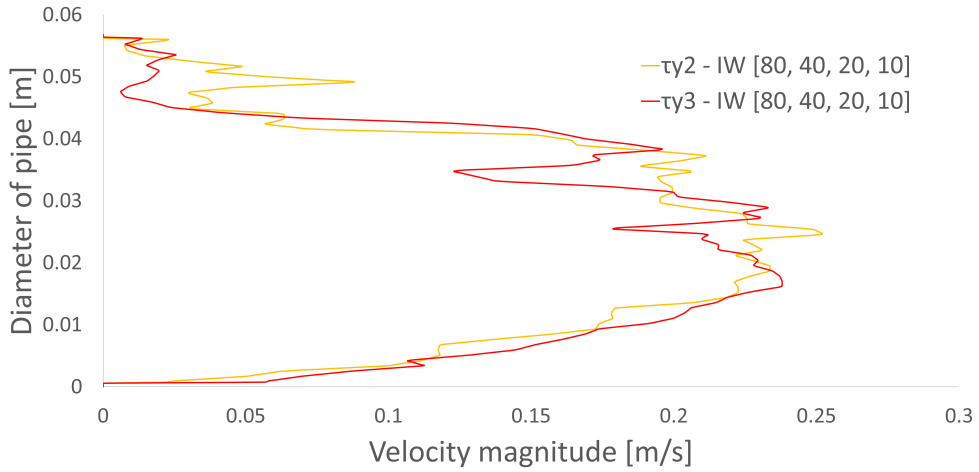

Figure A.4: Velocity magnitude of 0.8 g/L and 1.0 g/L with IWs 80→ 40 → 20 → 10.

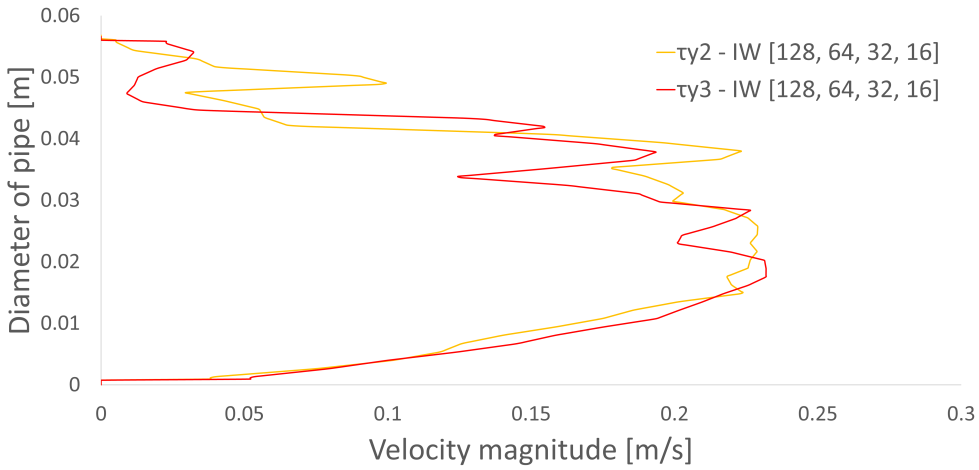

Figure A.5: Velocity magnitude of 0.8 g/L and 1.0 g/L with IWs 128→ 64 → 32 → 16.

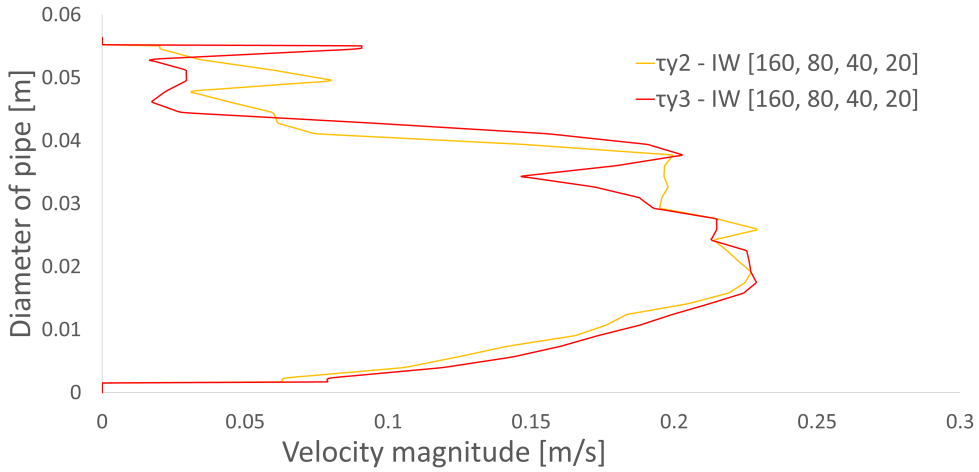

Figure A.6: Velocity magnitude of 0.8 g/L and 1.0 g/L with IWs 160→ 80 → 40 → 20.

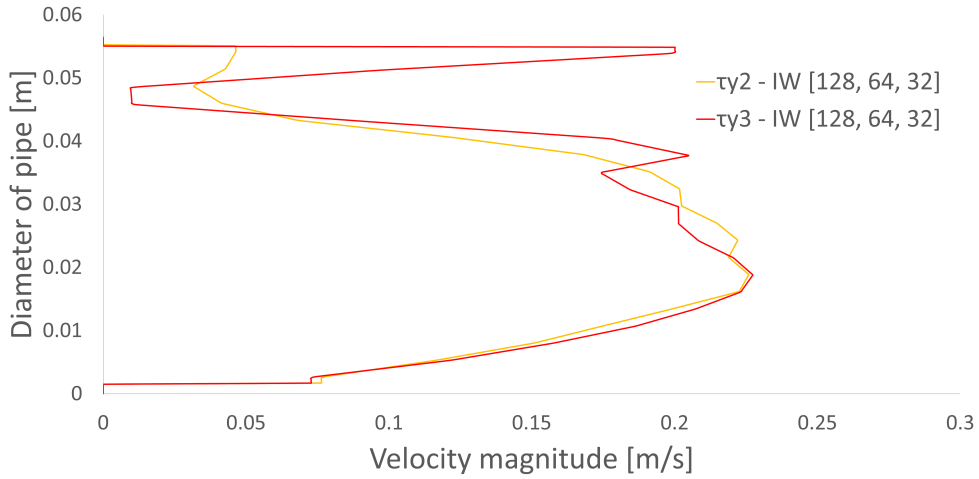

Figure A.7: Velocity magnitude of 0.8 g/L and 1.0 g/L with IWs 128→ 64 → 32.

The figures above are plots produced from different sized IWs. Only results for 0.8 g/L and 1.0 g/L are displayed, as more data points would make the differences harder to interpret. Like in section 4.3, the profiles for 0.8 g/L and 1.0 g/L are referred to as τ_2 and τ_3. Figure A.4 represents the initial settings that were also selected for the primary results. Multi pass with 50 % was used for all the models, with Figure A.5 from 128 to 16 pixels, Figure A.6 from 160 to 20 pixels and Figure A.7 from 128 to 32 pixels.

Newly obtained graphs were as expected somewhat cleaner than the first one. However, as the IWs gets bigger, increasingly large velocity spikes can be observed near the top of the pipe. These spikes are suspected to be false readings as it is present at the spot where the recordings are the blurriest. Additionally, a slight decrease of the peak velocity can be seen, which indicates loss of information through averaging of the flow.

Since the advantages of slightly less noise was decided to not justify the suspected false readings, the most detailed analysis from 80 to 10 pixels was used.

Additional tests were also carried out using the Image Pre-processing tool in PIVlab. By enabling "CLAHE" the contrast was enhanced, but the resulting velocity magnitude was almost indistinguishable from the initial results. As no attempt of enhancement was successful, the quality of the recordings was designated as the main problem.

Appendix B

Illustrations

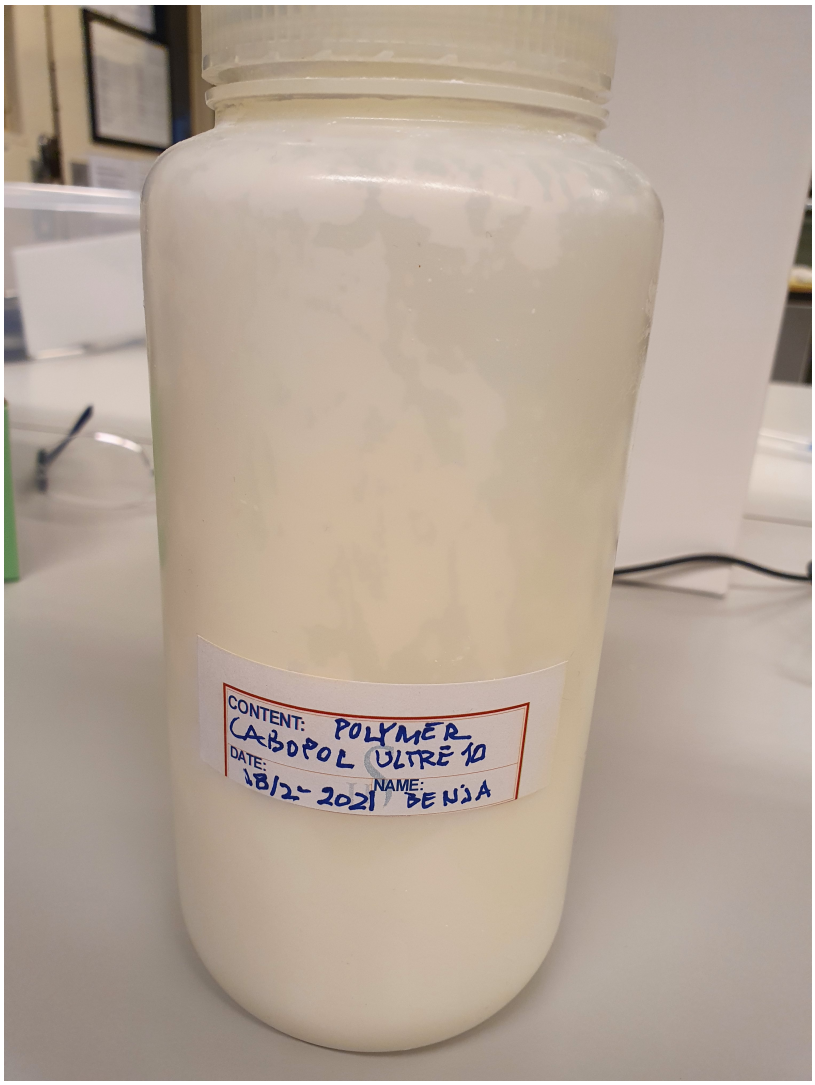

Figure B.1: Carbopol Ultrez 10, the polymer used for the viscoplastic fluids

Figure B.2: Mettler Toledo NewClassic MS, used to accurately measure Carbopol

Figure B.3: Mettler Toledo five easy

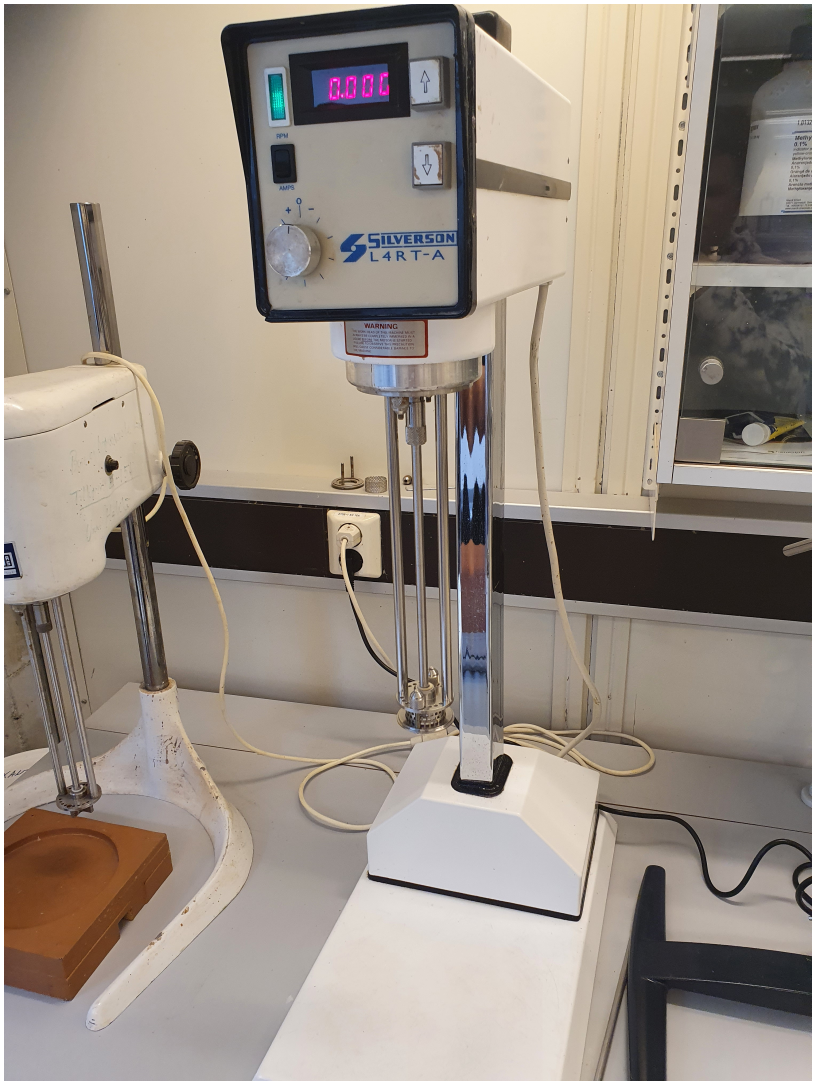

Figure B.4: Silverson L4RT-A, used to mix the fluids

Figure B.5: 8-speed viscometer model 800, the V-G meter used to study shear stress

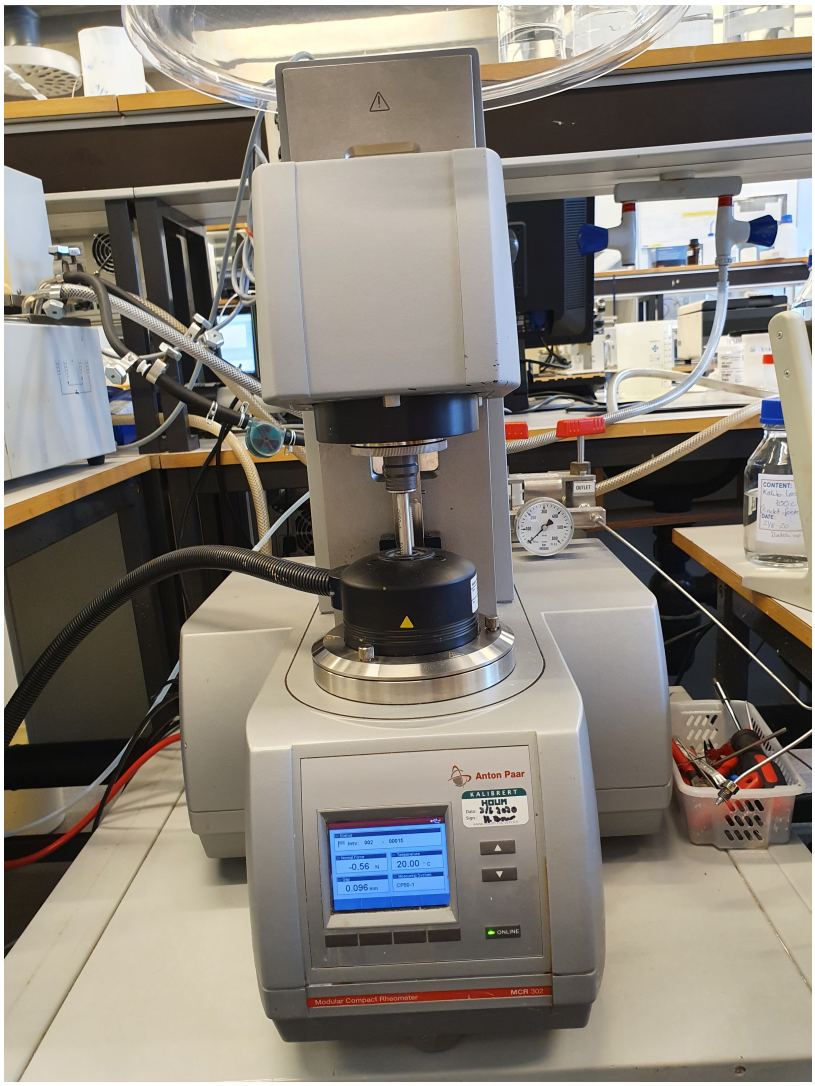

Figure B.6: Anton Paar Modular Compact Rheometer 302, used to carry out AS and a rotational test

Figure B.7: CP50-1, cone-plate used in MCR 302. Diameter = 50 mm, α =1°

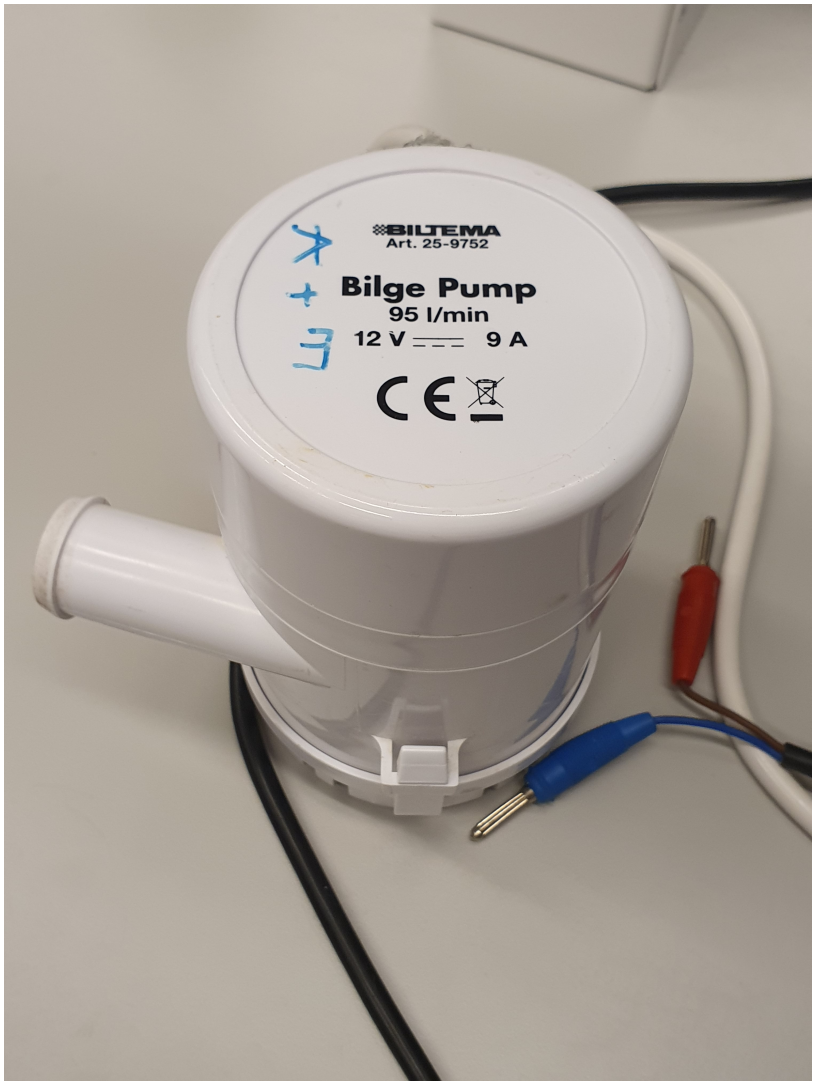

Figure B.8: Bilge pump 95 L/min, used to provide flow to the system

Figure B.9: Manson SP59602, served as a power supply

Figure B.10: Rosemount 3051 pressure transmitters. Nr 2 was faulty, Nr 1 measured pressure differences

Figure B.11: Cynergy^3 Ultrasonic Flowmeter, measured the flowrate for the system

Figure B.12: Flow straightener

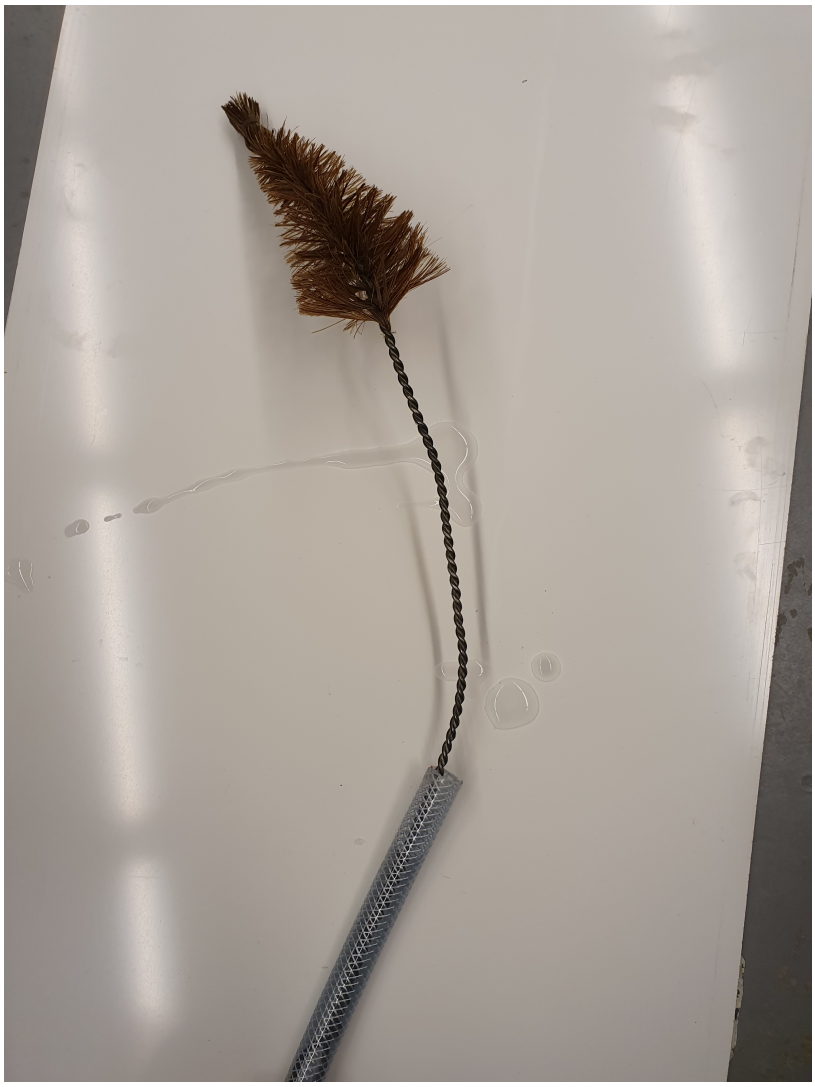

Figure B.13: conic pipe-brush, used in between PIV measurements to remove air bubbles or seeding material inside pipe

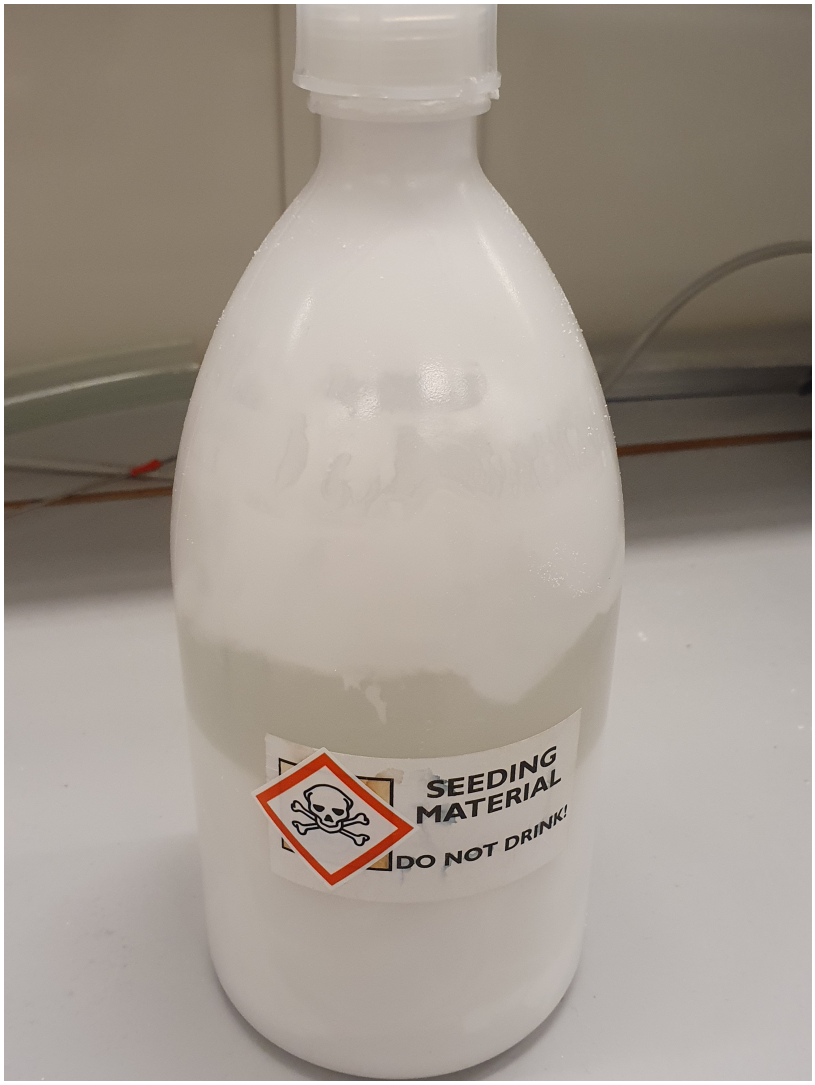

Figure B.14: Seeding material, was added to water for PIV measurements

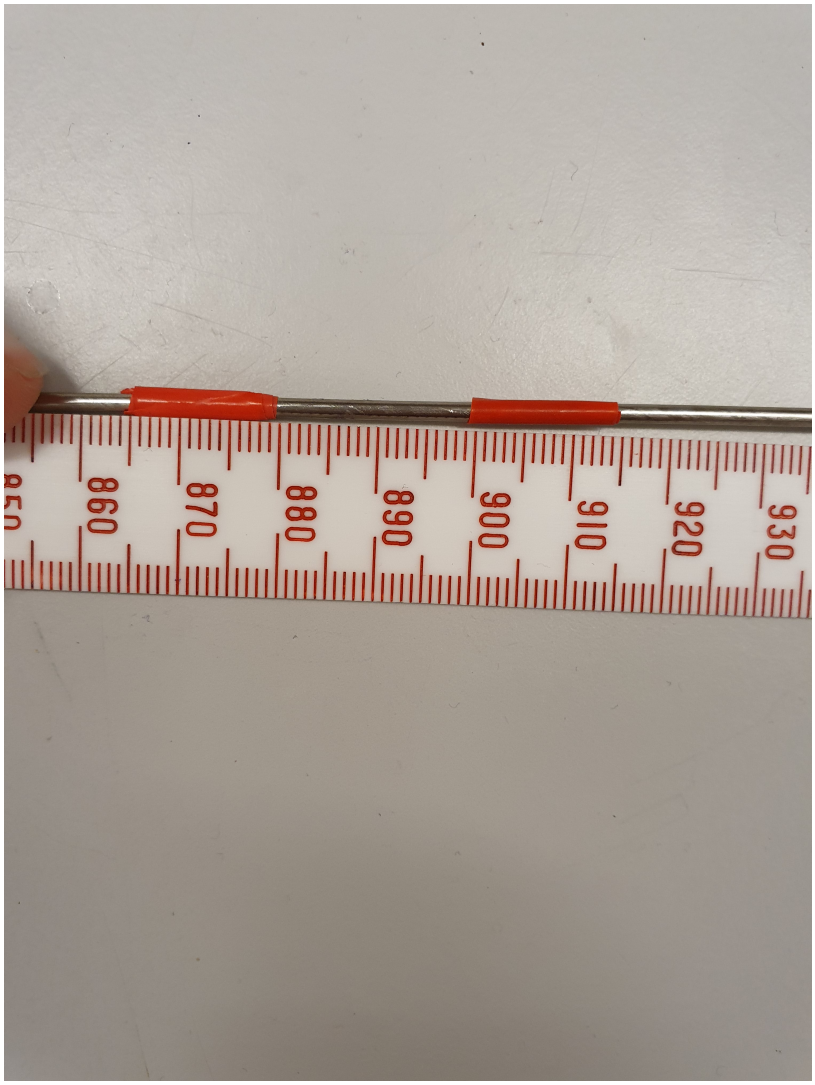

Figure B.15: Measuring calibration rod to 20 mm

Figure B.16: Basler Ace 510, used to carry out PIV measurements

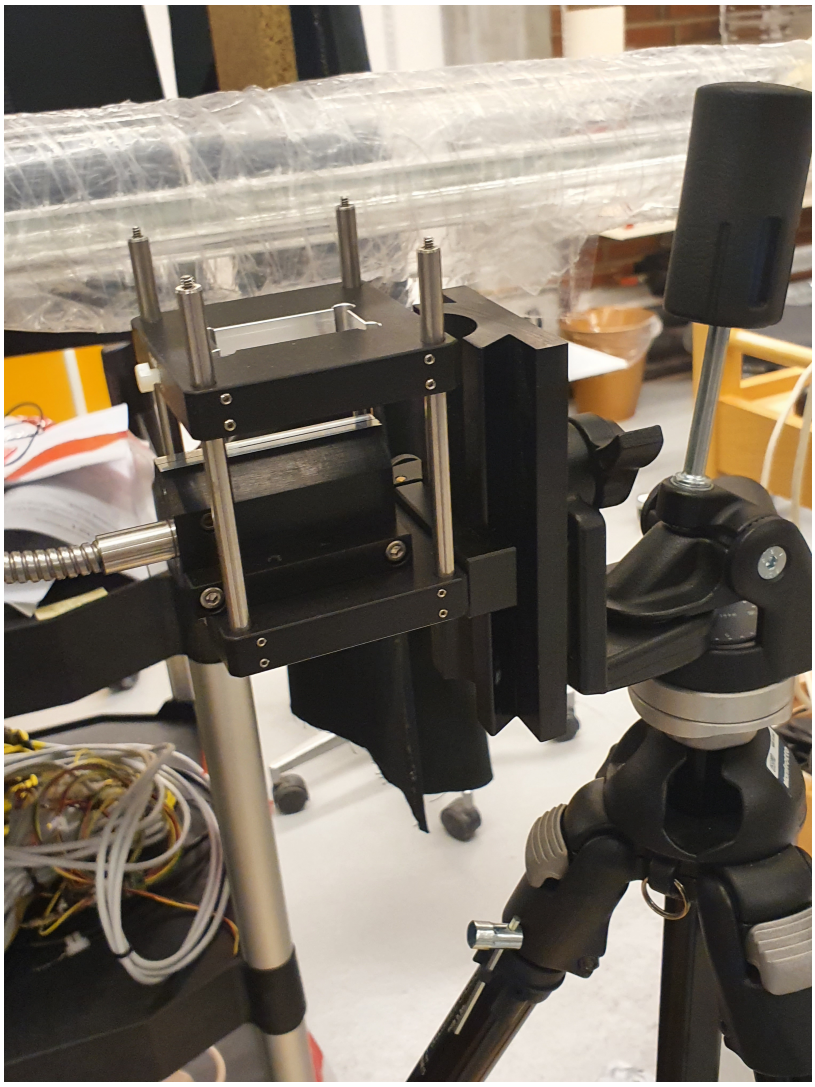

Figure B.17: LED Head-LPSv3, used to light up particles/air bubbles in fluid for PIV measurements

Figure B.18: Power supply for the LED